STRUCTURAL STUDY OF POLYGLUTAMINE AND MOLECULAR MECHANISM OF TOLL-LIKE RECEPTOR SIGNALING

A Thesis

by

ZHUYUN LIU

Submitted to the Office of Graduate Studies of
Texas A&M University
in partial fulfillment of the requirements for the degree of

MASTER OF SCIENCE

December 2008

Major Subject: Biochemistry

STRUCTURAL STUDY OF POLYGLUTAMINE AND MOLECULAR MECHANISM OF TOLL-LIKE RECEPTOR SIGNALING

A Thesis

by

ZHUYUN LIU

Submitted to the Office of Graduate Studies of
Texas A&M University
in partial fulfillment of the requirements for the degree of

MASTER OF SCIENCE

Approved by:

Chair of Committee,	Pingwei Li
Committee Members,	Dorothy Shippen
	Andreas Holzenburg
Head of Department,	Gregory Reinhart

December 2008

Major Subject: Biochemistry

ABSTRACT

Structural Study of Polyglutamine and Molecular Mechanism of

Toll-Like Receptor Signaling. (December 2008)

Zhuyun Liu, B.S., Nankai University

Chair of Advisory Committee: Dr. Pingwei Li

Huntington's disease (HD) is caused by the expansion of a CAG repeats encoding polyglutamine (polyQ) in the first exon of Huntingtin (Htt) gene. In HD patients, polyQ contains 36-183 glutamine residues, whereas normal individuals have a polyQ of only 8-35 residues. To elucidate this threshold phenomenon of polyQ aggregation, fluorescence proteins CFP and YFP were attached to both ends of polyQ of different lengths. FRET (fluorescence resonance energy transfer) was conducted to characterize the conformation of polyQ in the pre-aggregation state. Our FRET data show that both the normal and expanded polyQ tracts reveal the same extended structure in low concentration. Longer polyQ has multiple cooperative binding sites with higher avidity. PolyQ tracts form aggregates when proteins exceed a critical concentration. The antibody MW1 Fv fragment binds to polyQ, breaks apart polyQ oligomer and stabilizes it in a more extended conformation.

The addition of polyproline to the C-terminus inhibits polyQ aggregation by inducing PPII-like Helix structure. To understand how the flanking sequence affects the polyQ structure, the structure of Q10P10 peptide in complex with MW1 Fv was

determined by protein crystallography and compared with Q10/Fv crystal structure. Q10P10 peptide bound to Fv has a similar extended structure as Q10 peptide when a polyproline tract adopts PPII helical structure sticking out of the complex.

Toll-like receptors are transmembrane receptors on different kinds of leukocytes. They can recognize the structural conserved molecular motifs derived from microbes. On the upstream of the TLR signal pathway, TLRs recruit the adaptor protein-MyD88 through TIR/TIR domain interaction, and MyD88 recruits the downstream kinases IRAK4 and IRAK1 through death domain/death domain interaction. Pellino1, a newly identified E3 ubiquitin ligase, is also involved in TLR signaling by adding polyubiquitin chain to IRAK1 in conjugation with Ubc13/Uev1a E2 complex. TIR/TIR and DD/DD binding motifs were studied with techniques including mutagenesis, analytical gel filtration, NMR spectroscopy and crystallography. We identified a MyD88DD (E52QR62S) double-mutant that attenuates protein aggregation without interrupting the binding with IRAK4. This double mutant is a good candidate for structure determination by NMR spectroscopy. Our ubiquitination assay showed Pellino1 catalyzes polyubiquitination in the presence of Ubc13/Uev1a in vitro. Needle cluster-shaped crystals of Pellino1/Ubc13/ Uev1a protein complex were obtained by “hanging drop” method of vapor diffusion. Once the crystallization conditions are optimized, we will be able to collect X-ray diffraction data for this E2/E3 complex.

ACKNOWLEDGEMENTS

I appreciate the generous guidance and assistance from my graduate committee. I would like to thank my advisor Dr. Pingwei Li. He is always there to meet and talk about the research project, to review and proofread my thesis. He did not give up on me after I decided to pursue my professional life in a different direction. Thanks also go to Dr.Shippen, Dr. Holzenburg and Dr. Sacchettini for their endless encouragement and support in developing new ideas and for trouble shooting.

I would also like to say "thanks" to the following people: Dr. Xiaojun Li, who provided tremendous technical support in the past three years; Cheng Lv, who helped preparing experiments; Dr. Chapman from the University of Wisconsin, who gave me the CFP and YFP construct as a generous gift; and Dr. Kao, who provided the Perkin Elmer LS55 for FRET experiments.

I also want to extend my gratitude to my friends, colleagues and the department faculty for making my time at Texas A&M University a great experience.

Last, but not least, thanks to my mother and father for their great love. They have been my source of fulfillment, inspiration and joy through out my life.

NOMENCLATURE

AUC	Analytical UltraCentrifugation
CD	Circular Dichroism
CFP	Cyan Fluorescence Protein
DD	Death Domain
DRPLA	DentatoRubral and PallidoLuysian Atrophy
FRET	Fluorescence Resonance Energy Transfer
HD	Huntington's Disease
HSQC	Heteronuclear Single Quantum Correlation
Htt	Huntingtin Protein
IL-1R	Interleukin-1 Receptor
IRAK	IL-1R-Associated Kinase
MyD88	Myeloid Differentiation Gene 88
polyQ	Polyglutamine
SBMA	Spinal and Bulbar Muscular Atrophy
SCA	Spino-Cerebellar Ataxia
TLR	Toll-like Receptor
TIR	Toll/Interleukin Receptor
YFP	Yellow Fluorescence Protein

TABLE OF CONTENTS

LIST OF FIGURES

FIGURE Page

LIST OF TABLES

CHAPTER I

INTRODUCTION

Structural Study of Polyglutamine

Huntington's disease and Huntingtin protein

Huntington's disease is a genetic neurological disorder. It results from the programmed degeneration of neurons in a certain area of brain (Figure 1).The patients show symptoms including uncontrolled movement, slurred speech, depression and loss of cognitive function. More than 15,000 Americans have Huntington's disease, while at least another 150,000 have 50 percent risk of developing the disease, and thousands more of their relatives live with the possibility of late onset of Huntington's disease (data from NINDS). Currently, there is no cure for Huntington's disease, but some treatments can reduce symptoms and prevent complications.

Huntington's disease was first described by the physician George Huntington in 1872, but the gene associated with the disease was not discovered until 1993 (HDCRG, 1993). Huntingtin (Htt) gene encodes a 346 kD protein of unknown function. Htt protein is widely expressed in human tissue all over the body (Dure et al., 1994), and the expression level is the highest in the brain, especially in cerebellum followed by the cortex, striatum, hippocampus and olfactory lobe (Landwehrmeyer et al., 1995). In mice, deletion of Htt gene causes early embryonic lethality, whereas later null mutation of Htt results in neuronal degeneration (Dragatsis et al., 1998; Duyao et al., 1995; Nasir et al., 1995; Zeitlin et al., 1995).

Investigations on Htt protein's exact function have hinted at its role as a scaffold protein that interacts with many proteins, including splicesome, transcription complex, and signaling proteins (MacDonald et al., 2001; Jones, 2000). The entire 350 kD protein have a 36 tandem "α helix-loop-α helix" motif stacking together to form a curvature to foster the protein-protein interaction or RNA-protein interaction (MacDonald, 2003). Based on localization experiments, Htt protein is predominantly distributed in cytoplasm,

---

This thesis follows the style of the Journal of Neuroscience.

but it can shuttle between nucleus and the cytoplasm. Therefore it is also likely to involve with cytoskeletal function or vesicle transportation (Ross, 2002).

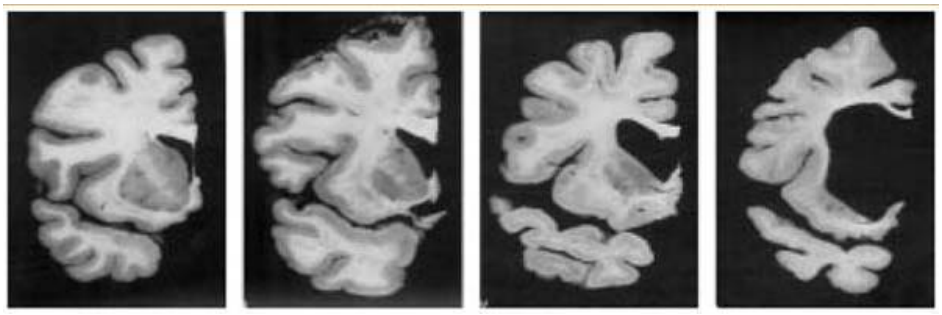

FIGURE 1. Neuropathology of Huntington's disease in postmortem brain. Brain mass loss with the increasing severity of disease (from left to right). (http://www.buckinstitute.org/site)

Polyglutamine pathogenesis

The first exon of Htt gene contains a repeated CAG region encoding polyQ tract (Figure 2). The number of glutamine residues may vary among different individuals. In HD patients huntingtin contains 36-183 glutamine residues, whereas the normal individuals have a poly Q tract of only 8-35 residues (Rubinsztein et al., 1996; Sathasivam et al., 1997). The disease severity and the early onset are closely related to the length of the polyQ tract. The children of the HD patient usually suffer from more severe symptoms and earlier onset because of the CAG repeat expansion during oogenesis and spermatogenesis.

The molecular mechanism for the correlation between polyQ and the disease progression remain unclear. A common feature of neurodegenerative diseases caused by polyQ expansion is the formation of inclusion bodies in affected brain regions. Electron

microscopy images of brain sections reveal that neuronal inclusions of mutant huntingtin protein show fibrilla morphology (Scherzinger et al., 1997). Similar neuronal inclusions of aggregated protein were observed in other polyglutamine diseases, including SBMA, DRPLA and SCA.

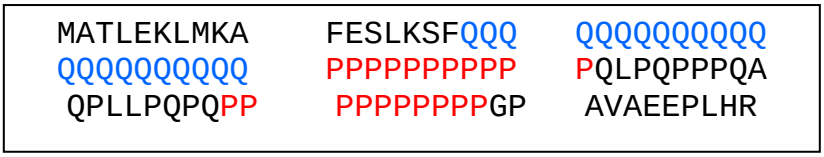

FIGURE 2. Amino acid sequence of HD exon 1 with 23 glutamines. The polyglutamine region is highlighted in blue, and the polyproline regions are highlighted in red.

Here is a widely accepted mechanism for the formation of amyloid fibril from elongated polyQ tract (Figure 3). When a polyQ is within the pathological range (>37 glutamines), the elongated polyQ tract is transformed from a random coil structure into a "toxic fold", which is rich in β-sheet structure. Then dimers, trimers and larger oligomers are formed during a lag time. After the protein concentration exceeds a critical value, unstable nuclei are slowly forming. Once cross the threshold of nucleation, the fibrils formation becomes thermodynamically favorable and leads to rapid grow of amyloid fibrils. It is commonly assumed that the expanded poly Q tract with an altered protein conformation gives rise to aberrant binding interactions with other cellular proteins, such as transcription factors, heat shock proteins, ubiquitin and proteasome components, leading to protein aggregation and sequestration.

However, other studies indicate that protein aggregation is not the main cause of cellular toxicity. Conversely, it has been suggested that the aggregates could represent a cellular protective response by which the cells try to degrade the toxic expanded protein

(Masino and Pastore, 2001). In order to solve this paradox, a better understanding of the structural features of the polyQ tracts will be crucial to unraveling the mechanism of polyglutamine pathogenesis.

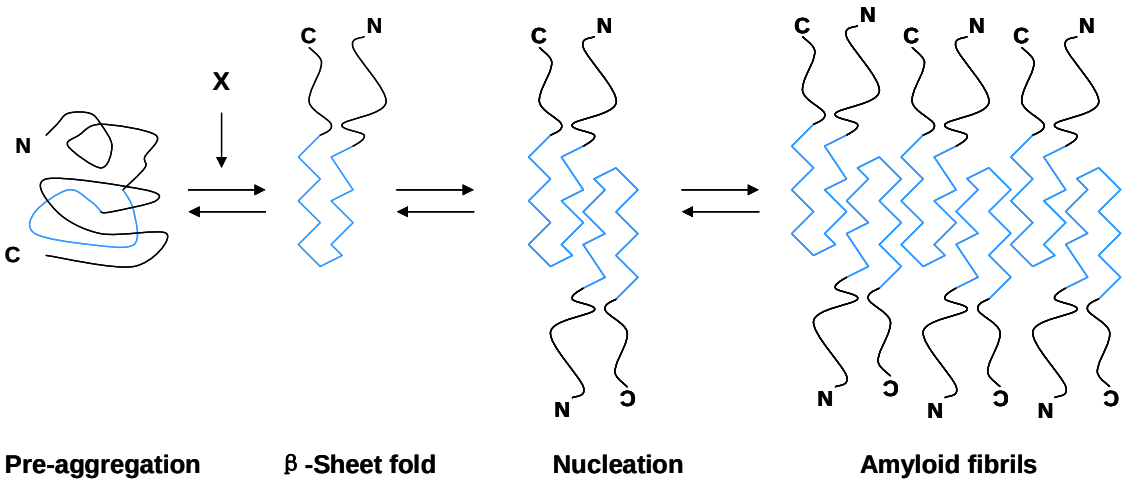

FIGURE 3. Mechanism of protein aggregation from elongated polyQ. Blue, polyQ tract (>37 glutamines); black, other amino acid sequence in Htt protein. X, unknown proteins such as transcriptional factors, chaperons, proteases.

Models of polyglutamine tracts in solution

There are several models to characterize the structural features of polyQ stretches in solution by the methods of molecular modeling. It was proposed that long stretches of polyQ could form antiparallel β-strands through hydrogen bonds and further assembled into β-sheets or β-barrels (Perutz et al., 1993). A slightly different model suggested random coil to β-hairpin transition for a poly Q tracts comprising more than 40 glutamines (Starikov et al., 1999). Lathrop came up with four possible motifs for poly-Q repeats: parallel and antiparallel β-sheet, α-helix and π-helix (Lathrop et al., 1998)

Experiments were carried out to test these models. The results of CD experiments indicate that normal polyQ tracts (Q9-Q17) are in a random coil structure, whereas solid phase Fourier-transform infrared spectroscopy showed controversial results (Sharma et al., 1999): polyQ tracts are in a β-sheet structure rather than in a random coil structure. Recent experimental data suggested that polyQ peptides may adopt the left-handed polyproline II helix structure (Chellgren et al., 2006; Wang et al., 2006).

PolyQ specific antibodies are useful tools for probing the structure of polyQ

The study of the polyQ structure is hampered by its flexibility and insolubility. The crystal structure of bovine ribonuclease A with GQ10G insertion in the hinge loop shows that polyQ region is unstructured (Sambashivan et al., 2005). Polyglutamine repeats inserted in a dimeric chymotrypsin inhibitor 2 also show disordered structure (Chen et al., 1999). The generation of several polyQ specific antibodies, such as MW1, 1C3, 3B5H10, provides a new way to determine the polyQ structure. Our lab developed a strategy to "fix" the flexible polyQ tract by embedding it in the specific antibody MW1 and solved the crystal structure of Fv-GQ10G complex. The GQ10G peptide lies in a diagonal groove of MW1 Fv (Figure 4B). It adopts an extended structure of about 29 Å long, while six out of ten glutamine residues adopt polyproline II helical structure and three others adopt a β-strand structure (Figure 4A). These observations agree with the results from the previous computer modeling, CD and spectroscopic experiments (Li et al., 2007).

Although crystallography studies of polyQ in complex with MW1 represent a feasible approach to probe the structure of soluble polyQ, it also raises the questions: Does the structure of the bound polyQ really reflect the structural features of free polyQ in solution? Or MW1 induces the conformation change of free polyQ via hydrogen bonds and van der waals interactions to fit the polyQ tract into its preexisting groove? New approaches should be applied to monitor the conformation change of the polyQ tract upon the binding of MW1 Fv.

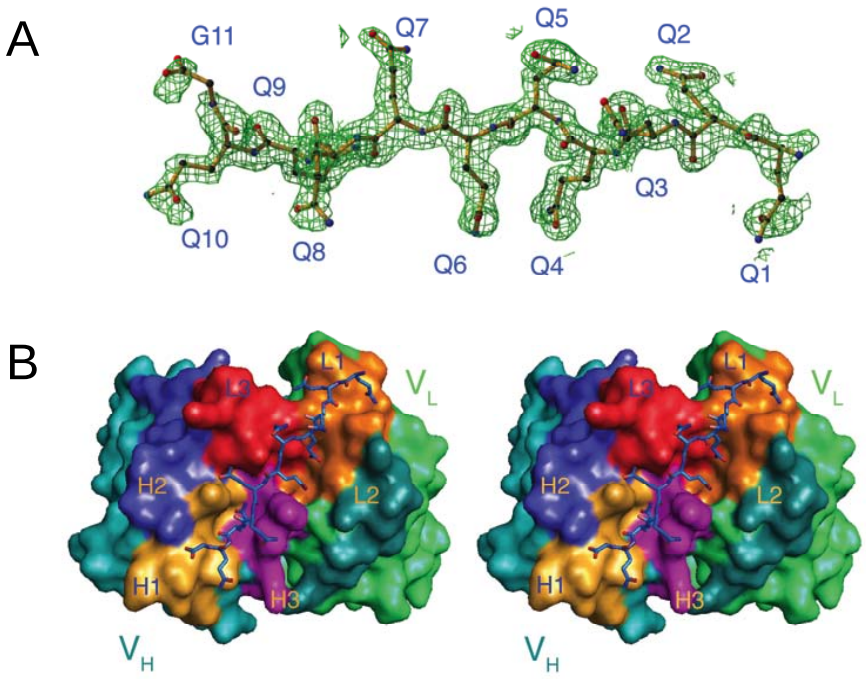

FIGURE 4. Structure of $polyQ_{10}$ peptide bound to MW1 Fv. (A) The GQ10G peptide model superimposed on a 1.68 Å annealed omit electron density map contoured at 0.9 σ. (B) Stereo surface representation of $polyQ_{10}$ peptide binding site in MW1 Fv. Peptide is shown in blue stick model (from Li et al., 2007).

Linear lattice model of polyQ

The antibody MW1 we used was generated by Paul Patterson in California Institute of Technology. Epitope Mapping shows MW1 binds specifically with polyQ tract in Htt exon1. It is clear that MW1 bind the expanded polyQ (>36 glutamines) form of Htt far more strongly than normal Htt. A widely accepted paradigm to explain this phenomenon is that the expanded polyglutamine repeats undergo conformational changes and thus preferentially bind with MW1 antibodies. A recent solution NMR study of polyglutamine tracts in GST fusion protein by Masino et al. challenged this paradigm. They claimed that both the normal polyQ tract (22Q) and expanded polyQ tracts (41Q) adopt a random coil structure and no differences were observed between GST-Q22 and GST-41Q in NMR spectra.

A new linear lattice model was proposed by Bennet et al. to explain the paradox between preferential targeting of expanded polyQ tracts by MW1 and the same random coil structure in normal and expanded polyQ tracts (Figure 5). In this model, polyglutamine is a linear array of n repeating units. A monovalent MW1 binds to 9 glutamine residues. A multivalent antibody can bind with a longer polyQ by interacting with two or more binding sites simultaneously. The positive cooperativity of the multiple binding sites significantly increases the binding affinity. The pathological threshold observed in HD is not related to a global conformation change from a soluble, random coil structure of polyQ tract to a pathological conformation. Instead, the increased number of binding sites of polyQ tract gives rise to the high binding affinity and cause the aberrant interaction with other proteins, leading to their functional dysregulation. It will be interesting to test this linear lattice model: whether the expanded polyQ tract adopt an extended conformation similar to short polyQ peptide or a conformation change occurs in polyQ above the pathological threshold of 36 glutamines.

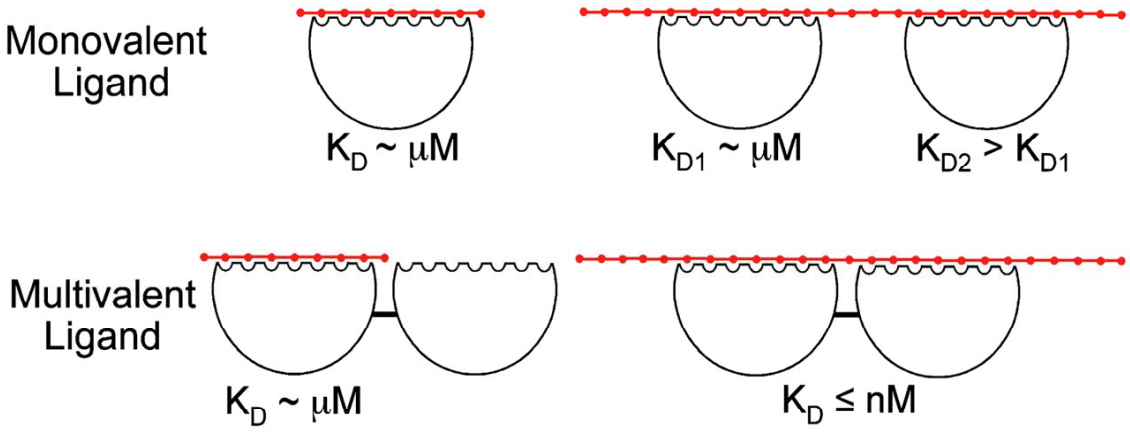

FIGURE 5. Linear lattice model for polyQ. PolyQ is a linear array of n repeating units (red dots), which adopts an extended structure accessible by multiple copies of ligand. A multivalent ligand can bind with high avidity by interacting with two of more binding sites simultaneously, thus distinguishing normal and pathologic polyQ (from Bennet et al., 2002).

Flanking polyproline sequence changes polyQ conformation

While the work on the structure of polyQ tract is still in progress, recent research started to focus on the protein context of polyQ repeats, especially its flanking regions. HD exon1 carries a sequence encoding for the human polyproline tract that lies adjacent to polyglutamine tract in Huntingtin. Polyproline motifs are responsible for Huntingtin interaction with SH3- and WW-domain-containing proteins, such as epidermal growth factor receptor (Liu et al., 1997), vesicle trafficking proteins (Qin et al., 2004), splicesome and transcriptional factors (Faber et al., 1998; Passani et al., 2000; Sittler et al., 1998), and they may be important to fully understand the interaction of mutant huntingtin with various proteins. Furthermore, the polyproline region is likely to confer structural stability to the Htt exon1. Wetzel and colleagues found that the flanking polyproline can suppress mutant Htt fibril formation when it is attached to the C-terminal of polyQ tract (Bhattacharyya et al., 2006). Based on CD, EM and x-ray diffraction, Merdith and colleagues suggested the flanking polyproline sequence increases the threshold for polyQ aggregation and inhibits amyloid formation by inducing polyproline II like helical structure (Darnell et al., 2007).

More and more evidence show that the flanking polyproline has great influence in polyQ stability and structure. It is the driving force for us to study Q10P10 peptides. We speculated that the polyproline region might affect Q10 structure and even its binding with Fv.

Molecular Mechanism of TLR Signaling

Pathogen recognition and innate immunity

Human host are constantly exposed to the attacks of microorganisms in the environment. To survive the challenges, hosts have evolved protected systems to eliminate the invaded pathogens in the body. Human immune system consists of two major subdivisions: innate immunity and adaptive immunity. Innate immunity is the second line of defense after the pathogen cross the first line of surface barrier like skin and intestinal epithelia. Unlike adaptive immunity, which is based on clonal selection from a huge pool of lymphocytes bearing antigen-specific cell surface receptors, the innate immune system distinguish self and non-self by recognizing certain conserved molecular patterns of the microbial pathogens through limited number of germline-encoded pattern-recognition receptors (PRRs). Three families of PRRs have been described: Toll-like receptor (TLR) family, NOD-like receptors (NLRs) and RIG-like helicases (RLHs) (Akira et al., 2006; Meylan et al., 2006). Recognition of pathogen by these PRRs would leads to activation of signaling cascades involved in immune and inflammatory response.

TLR family and their ligands

TLR family is the first family of PRRs that is studied in detail. TLRs are integral membrane protein, which consist of the extracellular domain and the cytoplasmic domain. The extracellular domains are responsible for pathogen recognition and contain leucine-rich repeats, which usually form a horseshoe structure. The cytoplasmic domain shows high similarity to the cytoplasmic portion of the IL-1 receptor and was termed TIR domain. So far, 12 members of TLRs have been identified in mammals (Akira et al., 2006; Meylan et al., 2006; Takeda and Akira, 2005). TLR2 recognizes peptidoglycan in Gram-positive bacteria, while TLR4 recognizes lipopolysaccharide (LPS), which is a major component of Gram-negative bacterial cell wall (Takeuchi et al., 1999). TLR2 dimerizes with TLR1 or TLR6 respectively to discriminate the subtle difference between diacyl lipopeptides and triacyl lipopeptides. TLR3, TLR7 and TLR9 are located on the

endosome surface and responsible for the recognition of viral double stranded RNA, single stranded RNA and bacterial CpG DNA respectively (Alexopoulou et al., 2001; Heil et al., 2004; Hemmi et al., 2000). TLR5 have shown to be able to detect flagellin and mediate immune response to bacteria flagella (Hayashi et al., 2001) (Figure 6).

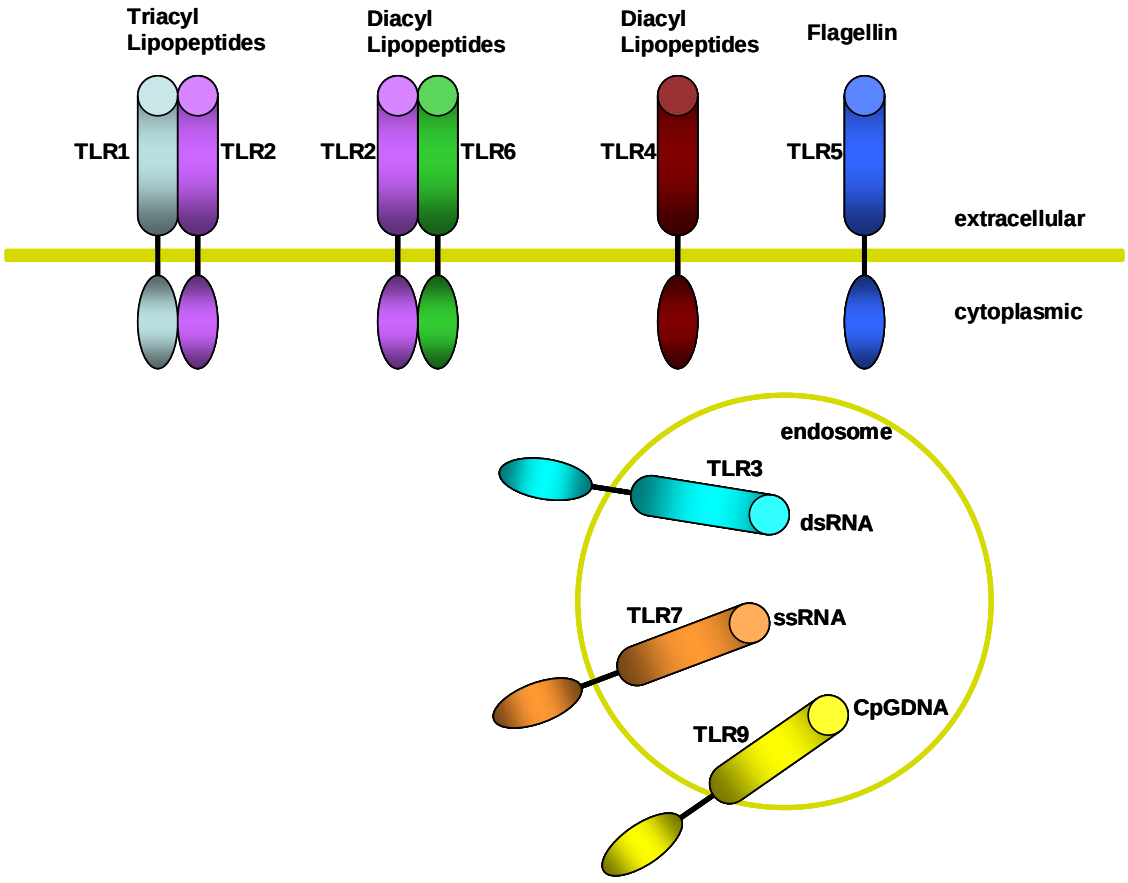

FIGURE 6. TLRs and their ligands (adapted from Takeda et al., 2005).

TLR signaling

Stimulation of TLRs by microbial pathogen activates signal cascades which involve the activation of transcription factor NF-κB and interferon regulatory factors IRF3, IRF5 and IRF7, resulting in the induction of proinflammatory cytokine genes (Akira et al., 2006). Many studies have been done in the recent year to elucidate the molecular mechanism by which TLRs trigger the signaling pathway.

TLRs and IL-1R share a similar intracellular signaling pathway in general. After ligand binding, TLRs dimerize and bring their cytoplasmic TIR domains to close proximity, which is important for the recruitment of adaptor protein MyD88 (Jin et al., 2007; Saitoh et al., 2004). MyD88 associates with TLRs through homotypic interaction of TIR domains and recruit the following IRAK4 (IL-1R-associated kinase 4) and IRAK-1 through homotypic interaction of death domain. IRAK4 phosphorylates IRAK1. Phosphorylated IRAK1 recruits TNFR-associated factor 6 (TRAF6) and subsequently form a complex of IRAKs, TRAF6 and Pellino1 (Schauvliege et al., 2007). TRAF6 acts as K63-linked E3 ubiquitin ligase and catalyzes polyubiquitination on itself in the presence of E2 ubiquitin-conjugating enzyme complex Ubc13/Uev1a (Deng et al., 2000). Then TRAF6 recruits and activates a complex containing TGF-β-activated kinase1 (TAK1) and the TAK1 binding proteins, TAB1 and TAB2. Activated TAK1 complex catalyzes the phosphorylation of IKK-β or activates MAP kinase cascade, resulting in the activation of NF-κB or AP-1 respectively (Wang et al., 2001). Pellino1 is a novel E3 ubiquitin ligase that induces K63-linked polyubiquitination of IRAK1 and thus degrades IRAK-1 by an unknown mechanism. This suggests that Pellino1 play an important role in down regulation of TLR signaling (Ordureau et al., 2008). (See Figure 7)

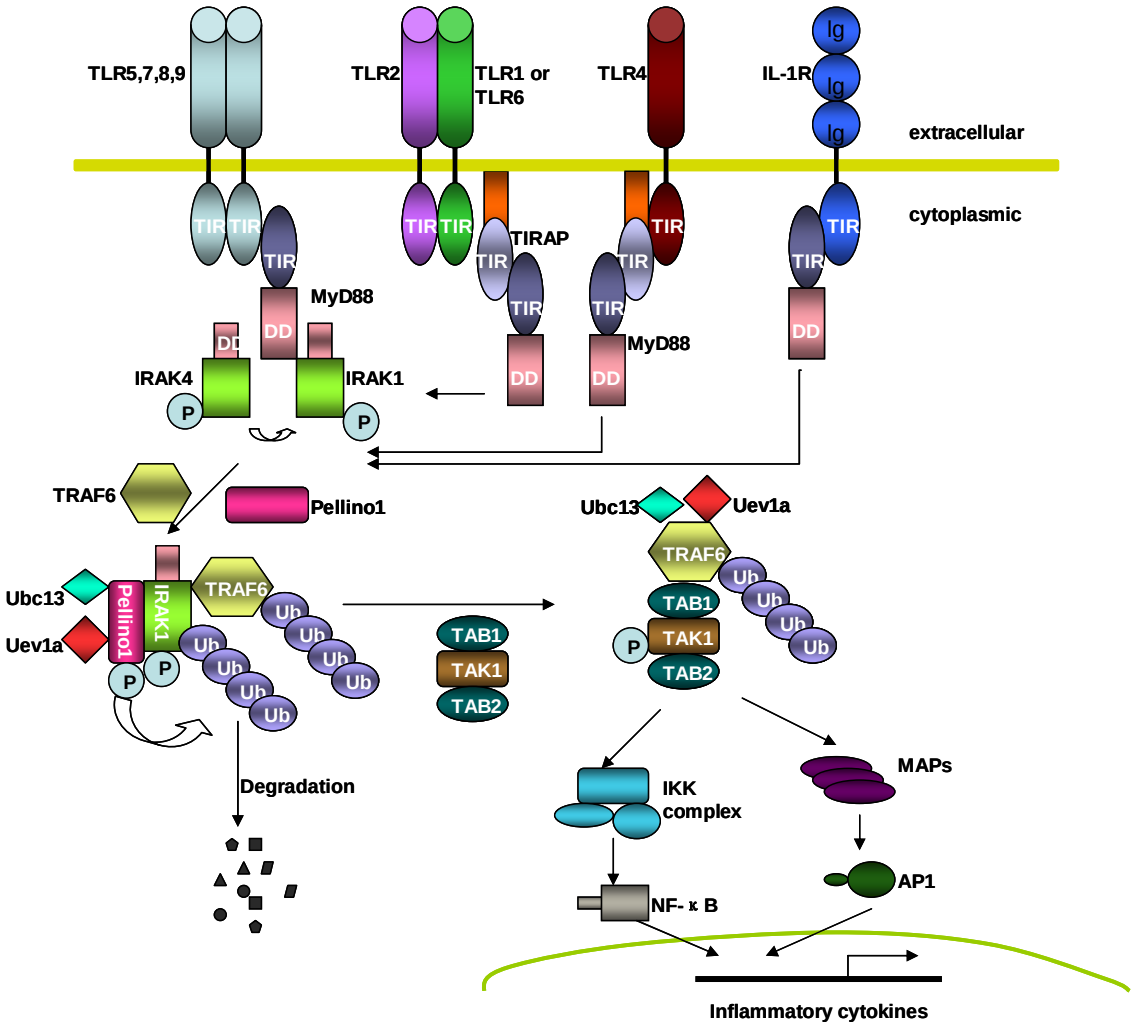

FIGURE 7.TLR/IL1-R signaling pathway.

MyD88 recruitment to TLRs

There are five human TIR-domain-containing adaptors: MyD88, TIRAP, TRIF, TRAM and SARM. Different TLRs use different combination of adaptors. MyD88 is a universal adaptor protein for TLRs signaling (O'Neill and Bowie, 2007). MyD88 was initially found in myeloid tissues and involved in the terminal differentiation of myeloid precursors induced by IL-6. MyD88 was first identified as adaptor protein in TLR signaling (Muzio et al., 1997; Wesche et al., 1997). Later MyD88's function in TLR signaling was further confirmed by studying MyD88 deficient mouse model (Kawai et al., 1999; Takeuchi et al., 2000). These mice do not show normal immune response upon the stimulation of ligands for TLR2, TLR4, TLR5, TLR7 and TLR9.

Human MyD88 encodes for a protein of 296 residues, containing an N-terminal death domain (DD, 1-110), a C-terminal TIR domain (155-296) and a short linker segment named as intermediate domain (ID, 110-155). MyD88 is recruited to TLRs via homotypic interaction of TIR domains. On the basis of protein sequence alignment, MyD88 TIR domain has 50 % similarity with TLR1 and TLR2 TIR domains (Figure 8). The canonical structure of TIR domain consists of five β-strands forming the core that is surrounded by five α-helices on both sides and five loops that connect between each β-strand and α-helix (Figure 9). Two conserved loops (BB loop and DD loop) are required for TIR dimerization between TLR1 and TLR2. BB loop of MyD88 has been shown to interfere with the interaction between MyD88 and IL-1R based on the docking model (Li et al., 2005), while the DD loop of MyD88 is responsible for the interaction between MyD88 and TLR2 (Xu et al., 2000; Dunne et al., 2003). This implicates that MyD88 might use distinct binding surfaces for different TLRs. Structural studies on the complex between MyD88 TIR and TLR TIR would be helpful to clarify this question.

```
BAD  AVG  GOOD

TLR1     NIPLEELQRNLQFHAFISYSGHDSFWVKNELLPNLEKE--GMQICLHERNFVPG
TLR2     ----------ICYDAFVSYSERDAYWVENLMVQELENFNPPFKLCLHKRDFIPG
MyD88    --PLGHMP--ERFDAFICYCPSDIQFVQ-EMIRQLEQTNYRLKLCVSDRDVLPG
cons        :.**:.*.  *  :*:  :: :**:  :::*: .*:.:**

TLR1     KSIVENIITCIEKSY-KSIFVLSPNFVQSEWCHYELYFAHHNLFHEGSNSLILI
TLR2     KWIIDNIIDSIEKSH-KTVFVLSENFVKSEWSKYELDFSHFRLFDENNDAAILI
MyD88    TCVWSIASELIEKRCRRMVVVVSDDYLQSKECDFQTKFALSL--S---PGAHQK
cons     . : .     ***   :  :.*:* ::::*: ..::  *:     .

TLR1     LLEPIPQYSIPSSYHKLKSLMARRTYLEWPKEKSKRGLFWANLRAAINIKLTEQ
TLR2     LLEPIEKKAIPQRFCKLRKIMNTKTYLEWPMDEAQREGFWVNLRAAIK------
MyD88    RLIPIKYKAMKKEFPSILRFITV---CDYT-NPCTKSWFWTRLAKALSL-----
cons      * **   :: . : .:  ::   ::. :. . :  **.*  *:.
```

FIGURE 8. Sequence alignment of MyD88, TLR1 and TLR2 TIR domain. T-COFFEE. (Version 6.07) Score=83.

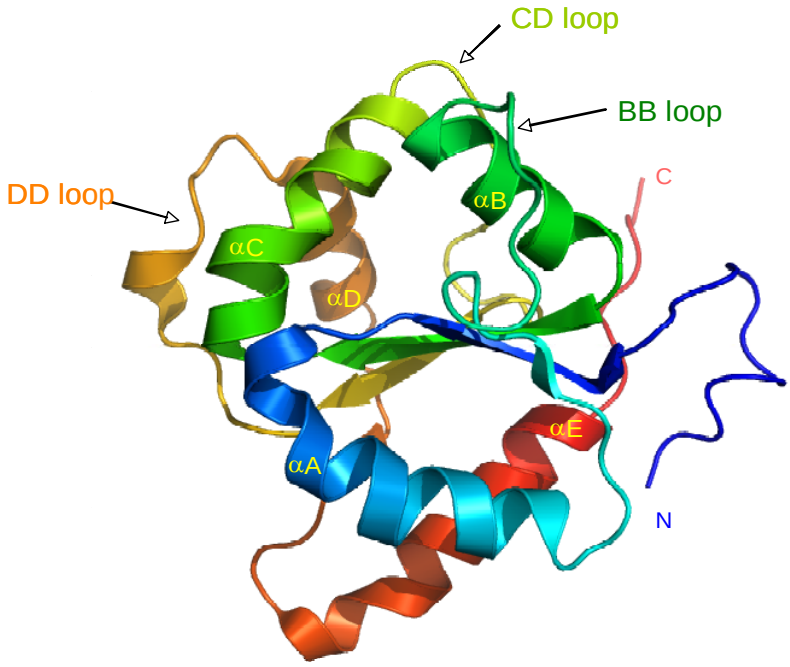

FIGURE 9. Crystal structure of TLR1 TIR domain (PDB ID: 1fyv).

MyD88 oligomerization

After MyD88 associates with TLR, this adaptor undergoes oligomerization to form a platform for the recruitment of downstream signal molecules. Over expression of MyD88 in HEK293 cells increases its oligomerization and results in robust NF-κB activation. Mutagenesis studies show that Box2 and Box3 of TIR domain constitute the interactive sites for MyD88 oligomerization (Li et al., 2005). Whether the death domain of MyD88 is involved in self-oligomerization remains unknown.

MyD88 brings IRAK1 and IRAK4 in close proximity and induces phosphorylation. MyD88 is the only adaptor in the TLR signal pathway that contains a death domain (DD). MyD88 recruits IRAK1 and IRAK4, which also have DD at the N-terminal through DD/DD interaction. The death domains play an important role in protein assembly in the NF-κB signal pathway, because they can activate their effectors via proximity- induced autoactivation, like trans-phophorylation in this case. To date, six structures of DD are solved with NMR spectroscopy or X-ray crystallography. All of them reveal a common feature of DD superfamily-the six-helical bundle structure with variation in length and orientation of the helices (Park et al., 2007a). Despites its significant biological function, only one DD/DD complex structure is available, which is Pelle-DD/Tube-DD in Drosophila. Pelle is homologous to IRAK4, but Tube has no counterpart in mammals. The crystal structure of the complex shows that the C-terminal tail of Tube fits within a groove of Pelle, suggesting a "Head to Tail" interface model (Xiao et al., 1999). (See Figure 10) In comparison, the death domain of IRAK4 shows a protruding loop in the groove, so a steric clash would happen if IRAK4DD and MyD88DD adopt the same "head to tail" interaction (Lasker et al., 2005). Either IRAK4DD has a different interface for MyD88DD, or IRAK4DD undergoes conformational changes to avoid the steric clash.

All these questions drive us to attempt to crystallize MyD88/IRAK4DD complex. A crystal structure of MyD88DD/IRAK4DD complex would shed light on DD/DD recruitment mechanism.

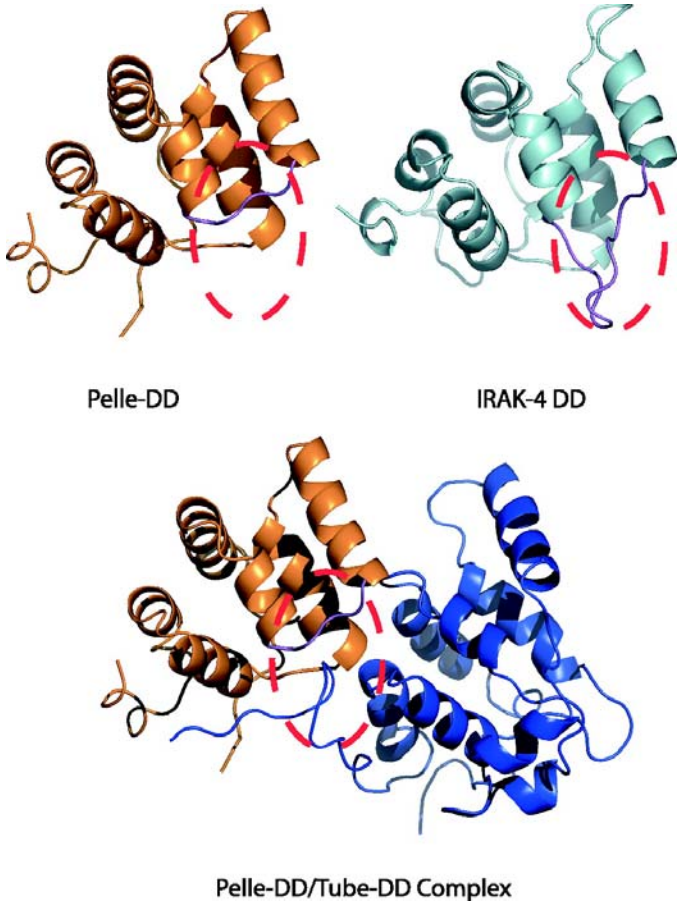

FIGURE 10. DD-DD complex structure (adapted from Lasker, M et al., 2005).

Ubiquitination in TLR/IL-1R

In addition to the roles TLRs play in innate immunity, they have also been characterized in dysregulated inflammation diseases. It is like a two edges weapon that you can use to protest yourself from microbial attack and also hurt yourself if it is used improperly. There must be a delicate molecular mechanism to turn TLR signaling on and off precisely.

Ubiquitination and de-ubiquitination of TLR network proteins were proposed to modulate TLRs signaling in accordance with the needs of host defenses (Lowe et al., 2006). For example, auto-polyubiquitination of TRAF6 allows for interaction with TAK1-TAB2 complex through binding of K63- linked polyubiquitin chain to the zinc finger domain of TAB2 and promote TAK1 auto-phosphorylation. Lately a new family of E3 ubiquitin ligase-Pellinos was found to involve in TLR signaling (Schauvliege et al., 2006).

In ubiquitination, target protein is covalently linked to one or more ubiquitin monomers. There are two common ubiquitin attachments: K48-linked and K63-linked. K48-linked polyubiquitin chain signals its substrate to 26S proteasome for destruction, while K63-linked polyubiquitin chain induces protein-protein interaction for DNA repair, endocytosis, and the stress response (Pickart et al., 2000). Both kinds of ubiquitin modification are catalyzed through the sequential action of three enzymes: E1 ubiquitin-activating enzyme, E2 ubiquitin-conjugating enzymes and E3 ubiquitin-protein ligase (Scheffener et al., 1995).

First, ubiquitin is activated by ATP and forms ubiquitin-adenylate intermediate. Then ubiquitin is transferred to E1 by forming a thioester linkage between the C-terminal carboxyl group of ubiquitin and E1 active site cysteine residue. Next, ubiquitin is transfer from E1 to the active site cysteine of E2. The final step is to convert ubiquitin chain from E2 to substrate with the assistance of E3. E3 enzymes are capable of interaction with both E2 and protein substrate and acts as the substrate recognition modules. (See Figure 11)

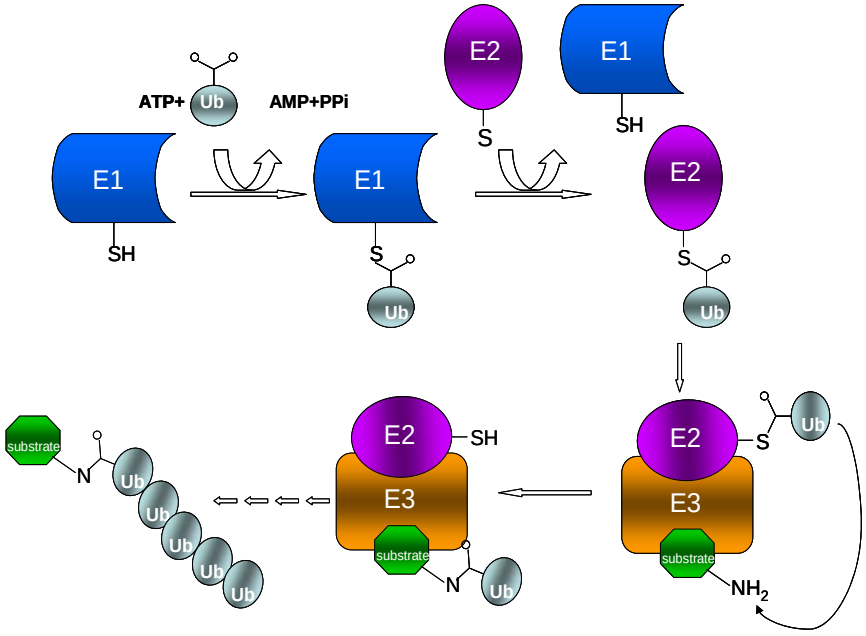

FIGURE 11. Mechanism of ubiquitination.

Pellino1 is E3 ubiquitin ligase

Pellino proteins had been proposed to function as scaffold proteins in TLRs signaling, because they bind with multiple proteins including TRAF6, IRAK1, IRAK4 and TAK1. Pellinos could be RING E3 ubiquitin ligase based on their primary sequence alignment (Schauvliege et al., 2006). All Pellino proteins contain an evolutionary conserved RING like domain at the C-terminal, which facilitates the direct transfer of ubiquitin from E2 to the target substrate (Figure 12). siRNA knock down of Pellino1 impaired IL-1 induced NF-κB activation.

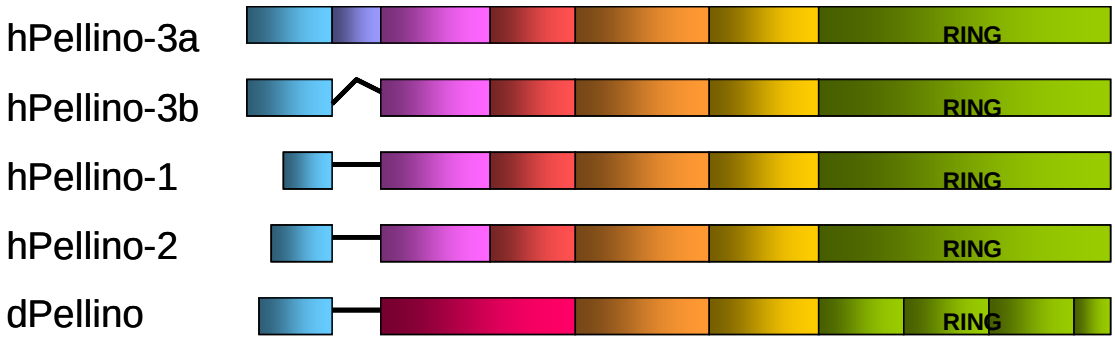

FIGURE 12. Schematic alignment of some representative Pellino proteins. Different exons of a particular Pellino are colored differently, and homologous exons in various Pellino sequences are marked in the same color. The RING domain in the C-terminus is indicated. (h)=human; (d) =Drosophila.

Recent publication have confirmed Pellino1 as E3 ligase (Ordureau et al., 2008). In vitro polyubiquitination experiments show that Pellino1, together with E2 conjugating complex Ubc13/Uev1a induce the formation of K63-linked polyubiquitination of IRAK1. K63-pUb-IRAK1 triggers downstream signaling events with unknown mechanism. It was proposed that K63-pUb-IRAK1 interact with NEMO-regulatory subunit of the IKK complex (NEMO has been shown to be capable of binding pUb chain specifically) and contribute to the activation of IKK β and NF-κB. Pellino1 in combination with another E2 conjugating enzyme UbcH3 catalyzes the formation of K48 pUb chains. We propose Pellino1 modulates the TLRs signaling by forming either K48 or K63 pUb linkage on IRAK1 in presence of different E2 ubiquitin conjugating enzymes. K48 linkage leads to IRAK1 degradation and switches off the TLR signaling pathway, while K63 linkage targets IRAK1 to IKK β complex and actives NF-κB. IRAK1 promotes reciprocal polyubiquitination of Pellino1 and leads to the degradation of Pellino1. It reveals a bidirectional regulation between IRAK and Pellino protein and suggests a novel mechanism for TLRs signal modulation.

E3 ubiquitin ligase contains a 70 residue RING finger bearing a set of cysteines and histidines which coordinate with two zinc atoms. RING domain mediates the interaction with the appropriate E2 enzyme and facilitates the direct transfer of ubiquitin from E2 to substrate (Pickart et al., 2001). Our lab determined the structure of Pellino1 and it shows that Pellino1 contains two CHC2 RING motifs and each of the two RING motifs binds one zinc atom. Docking of RING domain like of CHIP U-box to the structure of Pellino-1 shows that it is likely that first RING domain of Pellino-1 is involved in E2 binding. The second RING domain function remains unclear. This tandem arrangement of two RING motifs differs from all other known RING ubiquitin ligases, which generally contain a C3HC4 motif to coordinate with two zinc atoms. Compared with CHIP-UBC13-Uev1a complex and c-Cbl-Ubch7 complex, Pellino1 should adapt a different interaction motif with E2 (Zhang et al., 2005; Zheng et al., 2000). A crystal structure of E2/E3 complex will give us new insight into the mechanism of Pellino1 ubiquitination.

CHAPTER II

STRUCTURAL STUDY OF POLYGLUTAMINE

Objective

The importance of this polyglutamine tract is with no doubt, and lots of efforts have been exerted to understand how polyQ in the N-terminal of Huntingtin protein leads to pathologenesis in brain. The present study was inspired by the controversial models of polyQ raised by different research groups in the past decades. We studied the conformational differences between the normal and pathologic polyQ tracts in the pre-aggregation state. The structural changes that may occur after the addition of flanking polyproline were also investigated. Accordingly, we can reformulate the above objective to the following specific aims.

Specific aim 1: Testing the linear lattice model of polyQ

To test this model, we constructed a series of pET28 CFP (Cyan Fluorescence Protein) -Qn-YFP (Yellow Fluorescence Protein) expression vectors (n=10, 20, 37, 46) and measured the fluorescence intensity of CFP and YFP. FRET efficiencies and the distances between CFY and YFP were calculated. Data were analyzed to compare the conformation of normal and pathologic polyQ.

Specific aim 2: Monitoring the conformational change of polyQ upon binding of MW1 Fv

To resolve this issue, we monitored polyQ conformation change upon binding of MW1 Fv with FRET. Due to the high insolubility of pure polyQ stretches in aqueous solvents, in the previous studies, the peptides have been flanked by charged residues, or have been studied under extreme and non-physiological condition, such as low pH or organic solvents. Here we attached CFP to the N-terminus of the polyQ peptides and YFP to the C-terminus. If there is conformational change upon the binding of Fv, FRET

efficiency would change correspondingly. Our system has the advantages of studying the peptide in protein context and preventing the peptide from aggregation.

Specific aim 3: Probing the molecular structure of Q10P10 with antibody

We postulated that the flanking polyproline would affect the structure of polyQ tract by inducing PPII helix like structure. To gain further insight into the molecular structure of Q10P10 peptide, we crystallized Q10P10 peptide in complex with MW1 Fv and solved the structure by molecular replacement. Previous structure of polyQ was studied using GQ10G peptide, and thus did not take into account the possible effects of the flanking region on the physical properties of polyQ stretches. This study will advance our understanding about the pathologenesis of CAG expansion diseases and provide an alternative approach for potential drug design.

Experimental Procedures

Prepare CFP-X-YFP expression vectors

pECFP-C1 and pEYFP-C1 vectors are gifts from Dr. Chapman, University of Wisconsin. DNA primers were ordered from Integrated DNA Technologies (IDT). Primers were dissolved in ddH_2O to make a final concentration of 1 mg/ml. A typical PCR reaction was conducted using platinum Pfx kit (Invitrogen): 1 ul Pfx DNA polymerase, 1 ul each primer (1 mg/ml), 50 ng template, 2 ul MgSO4 (50 mM), 5 ul 10x buffer, 5 ul 10x enhancer, 1 ul dNTP (25 mM), ddH_2O to adjust to a total volume of 50 ul. The thermal cycle conditions are as follows: initial heating to 95 °C for 2 min, then 26 cycles of denaturing at 95 °C for 30 sec, annealing at 54 °C for 30 sec and elongation at 68 °C (1 kb per min), followed by cooling at 4 °C.

PCR products were confirmed by agarose gel electrophoresis and purified with PCR product purification kit (Qiagen, CA). Double restriction enzyme digestions were carried out for both the inserts and vectors as follows: 50 U each restriction enzyme (NEB), 5 ul 10x buffer, 100 ng vector or 300-1000 ng insert, ddH_2O to final volume of 50 ul, 37 °C for 5 hrs. Digested products were purified by agarose gel electrophoresis

and gel purification kit (Qiagen, CA). Ligation was carried out at room temperature for 2 hrs with 4 ul insert (40-100 ng/ul), 4 ul vector(15-60 ng/ul) and 1 ul T4 ligase and 2 ul 10x ligase buffer (Invitrogen, CA).

CFP was inserted between NdeI and BamHI in pET28 vector, while YFP was inserted between HindIII and XhoI, resulting in pET28-CFP-YFP vector. Huntingtin exon 1 contains 16Q, 25Q, 37Q, 46Q were inserted into pET28-CFP-YFP vector using BamHI and HindIII sites. pET28-CFP-Qn-YFP (n=10, 20, 37, 46) and pET28-CFP-Q10P10-YFP were generated by primer walking to add 10 residues of glutamine or proline at a time. A stop codon was added at the C-terminal of YFP. All the expression vectors have been confirmed by sequencing (Institute of plant genomics and biotechnology, Texas A&M).

***E.coli* protein expression test**

pET28 expression vector containing proteins of interest were transformed into BL21 for protein expression. One colony was picked from the agar plate and inoculated to 3 ml LB media with antibiotics in Falcon tube. It was incubated for 2-3 hr at 37°C by shaking at 250 rpm until OD_{600} reached 0.8. Cell culture was split into 3 x 1 ml LB: 1 ml saved as glycerol stock cells at -80°C, 1 ml with 0.8 mM IPTG added for expression test, 1 ml without IPTG as negative control. The last two were incubated for another 2 hours at 37°C and then harvested by centrifugation at 13,000 rpm for 1 min. Cell pellets were resuspended in 50 ul lysozyme buffer (0.2 mg/ml) and 1 ul DNase (1 mg/ml). Cells were lysed by 4 cycles of freezing in liquid N_2 and thawing at 37°C. Then cell lysate was spinned at 13,000 rpm for 2 min. Both supernatant and pellet were loaded on SDS-PAGE to check protein expression and solubility.

***E.coli* system protein large scale expression and purification**

50 ul glycerol stock cell was inoculated to 50 ml LB media with antibiotics and incubated until OD =1.0. 10 ml of start culture was transferred to each 1 L LB medium, and 0.6 mM IPTG was added when OD=0.8. Cell culture was shaken at 37 °C for 3 hrs.

Cells were spinned down at 6000 rpm for 10 min. Cell pellets were resuspended with Sonic Dismembrator (Model 500, Fisher Scientific) in 200 ml pre-chilled Tris-NaCl buffer (150 mM NaCl, 20 mM Tris, pH 7.5). Cell lysate was subjected to sonication again after adding 50 ul lysozyme buffer (50 mg/ml). Cell lysate sit on ice for 30 min, then was centrifuged down at 10,000 rpm for 15 min. Supernatant was further centrifuged at 16,000 rpm for 20 min at 4 °C to remove pellet completely. Supernatant was collected for Ni^{2+} column purification.

Ni^{2+} affinity chromatography and gel filtration chromatography

Cell lysate was mixed with Ni-NTA beads for 1 hr at 4 °C. Ni-NTA beads were spinned down at 4000 rpm for 2min and washed with wash buffer (10 mM imidazole, 150 mM NaCl, 20 mM Tris-HCl, pH 7.5) for 3 times. Protein was eluted with elution buffer (250 mM imidazole, 150 mM NaCl, 20 mM Tris-HCl, pH 7.5). Thrombin cleavage was conducted to cut off His-tag. Then protein sample was concentrated to 2 ml and loaded on Superdex 200/120ml column to remove His-tag.

Fv expression and purification

To generate a noncovalent MW1 Fv, the genes encoding the V_L domain and the V_H domain were subcloned into pET22b (+) (Novagen; San Diego, California, United States). pET22-V_L and pET22-V_H were transformed into BL21 and stored in 20% glycerol in -80 °C. V_L and V_H were expressed in 4 L and 2 L LB media separately at 37 °C for 4 hrs. Cells were harvested and resuspended in 200 ml pre-chilled lysis buffer (20 mM Tris, 100 mM NaCl, 5 mM EDTA, 0.5% Triton-X 100, pH 8.0). Cell lysate was subjected to sonication (60% amplitude) for 5 min to fully resuspend the cell pellets. 50 ul lysozyme buffer (50 mg/ml) and 50 ul Dnase buffer (10 mg/ml) were added into cell lysate and incubated at room temperature for 30 min for Dnase to digest genomic DNA. Inclusion bodies were spinned down at 8000 rpm for 10 min and resuspended in lysis buffer again by sonication of 2 min at 60% amplitude. This step was repeated 4 times to remove any impurity. Inclusion bodies were washed with 200 ml water to remove

detergent and centrifuged down again. Inclusion body pellets weighted about 0.8 g and were resuspended in 5 ml water by 20% amplitude sonication for 2 min. 7 M guanidine was added to denature the inclusion body. 20 mM GSH was supplemented to reduce the disulfide bond. The denatured proteins were centrifuged to remove aggregate protein. MW1 Fv was produced by the refolding the V_H and V_L inclusion bodies together at a molar ratio of 1:1 in 2 L refolding buffer (0.1 M Tris, 0.4 M arginine, 5 mM GSH and 0.5 mM GSSG). Several injections were made in two days to allow the slow refolding process of Fv protein. The refolding buffer was concentrated to 5 ml and exchanged to running buffer (50 mM Tris, 150 mM NaCl, pH 7.5). The refolded Fv fragment was purified by size exclusion chromatography (GE Healthcare, Piscataway, NJ, United States) and Ni-NTA chromatography as described before. The final yield of purified Fv was ~15 mg/L.

Fluorescence resonance energy transfer

Fluorescence Resonance Energy Transfer (FRET) is a one of the most useful techniques in monitoring conformational change of proteins. FRET takes place when a donor fluorophore in an electronically excited state transfers its excitation energy to a nearby acceptor fluorophore through resonance interaction. Resonance energy transfer is a non-radioactive quantum mechanical process that does not require a collision and does not involve production of heat. When energy transfer occurs, the acceptor molecule quenches the donor molecule fluorescence, and increases fluorescence emission of the acceptor. The phenomenon can be observed by exciting the protein containing both donor and acceptor molecules with light of wavelengths corresponding to the absorption maximum of the donor fluorophore, and detecting light emitted at wavelengths centered near the emission maximum of the donor and acceptor. An alternative detection method, growing rapidly in popularity, is to measure the fluorescence lifetime of the donor fluorophore in the presence and absence of the acceptor.

There are several criteria to be satisfied for FRET to happen. 1) The donor and acceptor must be within 10-100 Å of each other. 2) An appreciable overlap of the

emission spectrum of the donor with the absorption spectrum of the acceptor. 3) Fluorescence lifetime of the donor molecule must be of sufficient duration to permit the event to occur. The distance dependence of the resonance energy transfer process is the primary basis for its utility in investigation of conformational changes.

Fluorescence measurement

In general, we used 100, 200, 300 nM CFP-Qn-YFP fusion protein in a total volume of 1 ml Tris buffer (150 mM NaCl, 50 mM Tris, pH7.5). The emission spectra from 450-600 nm were scanned using Perkin Elmer LS 50 Spectrofluorimeter (Wellesley, MA). For each spectrum, sample was excited 3 times at 434 nm and scanned at 30-sec intervals. Protein concentrations were calculated based on the Trp absorption maximum at 280 nm (A_{280}) and extinction coefficient (ε_{280}): CFP-YFP fusion protein: 49530 $M^{-1}cm^{-1}$, CFP: 26025 $M^{-1}cm^{-1}$, YFP: 23505 $M^{-1}cm^{-1}$

Calculation of donor and acceptor apparent distance

Experimental data were analyzed using the Förster equation (Förster, 1948), which relates energy transfer efficiency (E) with distance (R) between donor and acceptor:

$$\mathbf{R^6=R_0^6(E^{-1}-1)} \qquad \textbf{Eq.1}$$

Where R_o, the Förster distance (in Å) at which the transfer efficiency is 50% and specific for a particular donor-acceptor pair, is defined as:

$$\mathbf{R_0=(J\kappa^2Q_0n-1)^{1/6}*9.7*103} \qquad \textbf{Eq.2}$$

The value of R_o depends on J, the spectral overlap integral; κ^2, the orientation factor for a dipole-dipole interaction; n, the refractive index of the medium between the donor and acceptor; and Q_o, the quantum yield of fluorescence of the energy donor in the absence of acceptor. The value of κ^2 cannot be directly measured and is the major uncertainty in the calculation of distance. Its value depends on the relative orientations of

the donor and acceptor dipoles; it is 0 if all angles are perpendicular and 4 if both transition moments are in line with the separation vector. Provided that both donor and acceptor can undergo unrestricted isotropic motion and rotate freely, κ^2 assumes a numerical value of 2/3. Dos Remedios and Moens (1995) argued that the assumption of a value of 2/3 for κ^2 appears to be valid for small peptides and small proteins. The CFP and YFP should have considerable motional freedom as they are attached to the rest of the peptide molecule via covalent single bonds. Assuming $\kappa^2 = 2/3$ and R_o=50 Å for the CFP and YFP pair (Patterson et al., 2001); these values were used in the calculation of distances.

As the presence of an energy acceptor in the vicinity of an excited energy donor provides an additional mode for the deexcitation process, from donor quenching, *E* is calculated from the equation:

$$E=1-I_{DA}/I_D \qquad \text{Eq 3.}$$

where I_{DA} is the fluorescence intensity of the donor in the presence of acceptor and I_D is the fluorescence intensity of the donor only.

Protein crystallization

Protein concentration was measure by its absorbance at 280 nm. Fv and Sumo-Q10P10 were mixed at a 1:1 molar ratio and concentrated to 15 mg/mL with Amicon Minipore. Protein sample was centrifuged at 15,000 rpm for 5 min at 4°C to remove aggregate before setting up hanging drop crystallization. About 200 crystal growing conditions were screened including Crystal Screen I & II and Index kit (Hampton Research, CA). Each microplate well was filled with 0.5 ml crystal growing solution. Then 2 ul of reservoir buffer was mixed with 2ul of protein sample on the center of coverslip. The well was sealed with grease to allow diffusion between hanging drop and mother liquid. (See Figure 13)

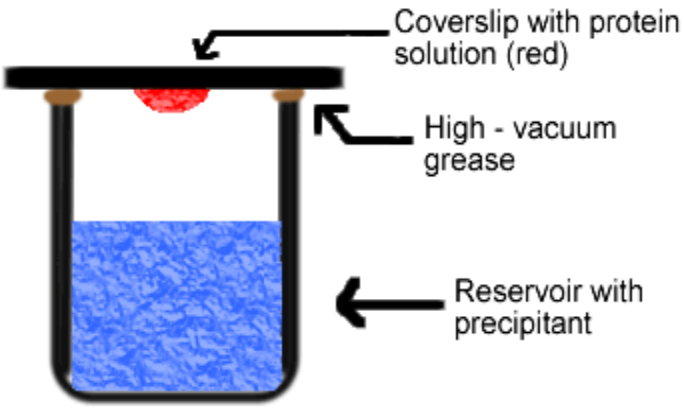

FIGURE 13. Protein crystallization by hanging drop.

Fv-Q10P10 structure determination

Further crystallographic studies were conducted with the MW1 Fv/Q10P10, which was crystallized in 50 mM Tris, 2.0 M $(NH_4)_2SO_4$ at pH 8.5. by the hanging drop vapor diffusion method. Crystals (space group P21 with two Fv molecules in the asymmetric unit) were cryo-preserved in liquid nitrogen in mother liquor containing 30% glycerol. Diffraction data from a single crystal were collected at -150 °C at beamline 8.2.2 (wavelength = 0.9537 Å) using a Quantum CCD detector at the Advanced Light Source (ALS, Berkeley). (The Advanced Light Source is supported by the Director, Office of Science, Office of Basic Energy Sciences, Materials Sciences Division, of the U.S. Department of Energy under Contract No. DE-AC03-76SF00098 at Lawrence Berkeley National Laboratory.) The data were processed with Denzo and Scalepack as implemented in the HKL2000 suite. The structure was determined by molecular replacement with MOLREP in the CCP4 suite using the search model of the Fv. Model building was done using O. The structure was refined using individual B factors and CNS. NCS restraints were not applied during the refinement since the two Fv molecules in the asymmetric unit had different packing environments.

Results

Spectral overlap between CFP and YFP

The most popular FRET pair for biological use is cyan fluorescent protein (CFP)-yellow fluorescent protein (YFP). Both are color variants of the green fluorescent protein. CFP and YFP can be easily attached to the host protein by molecular cloning. CFP-YFP pair saves the troublesome processes of chemical modification of organic fluorescent dyes. For FRET to occur, the emission spectrum of the donor probe must overlap considerably the absorption spectrum of the acceptor probe (Figure 14).

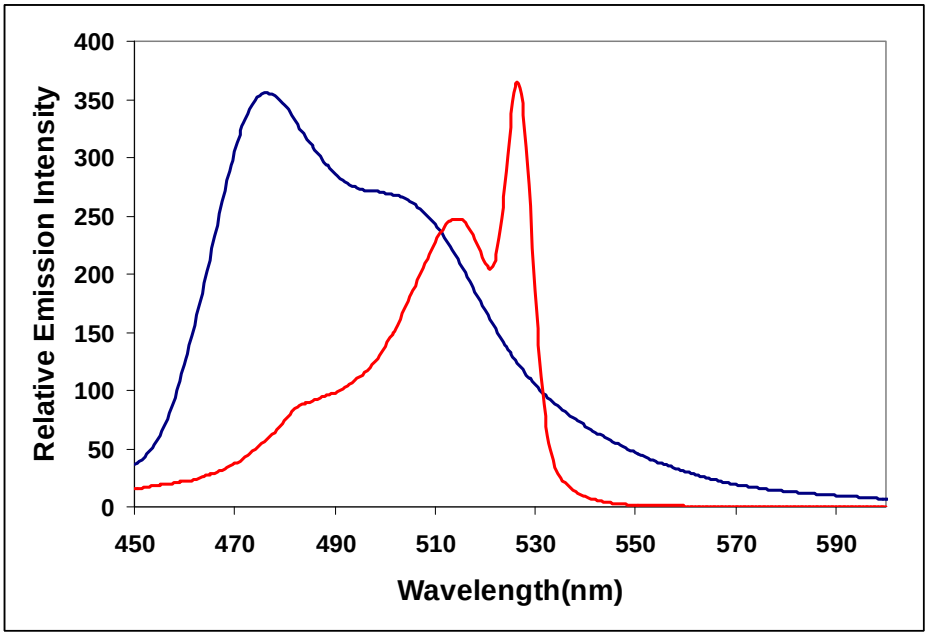

FIGURE 14. Spectral overlap of CFP and YFP. The corrected emission spectrum of 200 nM CFP (blue) and the absorbance spectrum of the 10 nM YFP (red) in Tris-HCl buffer.

Normal and expanded polyQ tracts adopt the same extended structure in solution.

Huntington Disease severity and the early onset are closely related to the length of the polyQ tract in the first exon of huntingtin gene. It is wide accepted that the expanded polyQ tract (>36) adopts a different conformation from the normal polyQ tract (8-35), which gives rise to the formation of a β-sheet structure and later on a nucleation process. However, our previous SPR binding experiments indicate that the antibody MW1 binds specifically with both the normal and expanded polyQ tracts. It was suggested that normal and expanded polyQ tracts adopt the same extended structure in solution.

To study the conformation of polyQ tract, we linked CFP and YFP together by peptides of n polyglutamine residues (n=10, 20, 37, 46). (See Figure 15A) If the CFP and YFP are close enough to each other, excitation of CFP moiety will result in the sensitized emission from the YFP moiety as a consequence of resonance energy transfer (Miyawaki and Tsien, 2000； Tsien, 1998). If the polyQ tracts adopt the same extended structure regardless of the number of glutamine residues, we expected to see a decrease in FRET efficiency with the increasing number of glutamine residues.

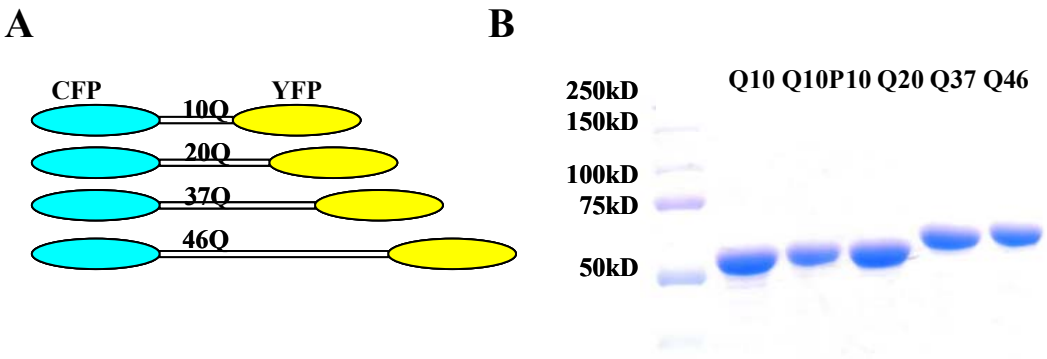

FIGURE 15. CFP-Qn-YFP fusion proteins. (A) Schematic representation of the CFP-Qn-YFP constructs. CFP and YFP were connected via a polyglutamine peptide. (B) Purified CFP-Qn-YFP fusion proteins on SDS-PAGE.

We measured the emission spectra of CFP-Qn-YFPs from 450-600 nm by PerkinElmer LS55 fluorometer. The excitation wavelength is 434 nm. The protein concentration is 300 nM in Tris-HCl buffer, pH 7.5. This concentration was chosen, because it is high enough to give fluorescence signal against the background while it is diluted enough to prevent the potential aggregation of polyQ tracts. There are two major peaks in the emission spectrum. One is CFP peak at 476 nm, the other one is YFP peak at 527 nm. All four CFP-Qn-YFP constructs can yield FRET signals (Figure 16). The CFP peak decreases while YFP peak increases correspondingly. CFP-Q10-YFP fusion protein has FRET efficiency of 37.9%. CFP-Q20-YFP fusion protein has a lower FRET efficiency of 27%. CFP-Q37-YFP and CFP-Q46-YFP fusion protein, which are above the threshold of normal polyQ tract in HD exon1, have FRET efficiency of 9.0% and 8.5%. Taking all the spectra into account, we suggested that the distance between N-terminal and C-terminal of polyQ tracts are determined by the number of glutamine residues. The data support the linear lattice model proposed by Bennett et al.. in 2002, in which HD exon1 fusion proteins with 16 to 46 glutamine residues reveal the same extended structures with random coil characteristics. FRET results reveal no global conformational change above 36 glutamines. FRET spectra excludes the possibility that expanded polyQ adopts the β-sheet model and bring the two ends of polyQ together to yield FRET signal.

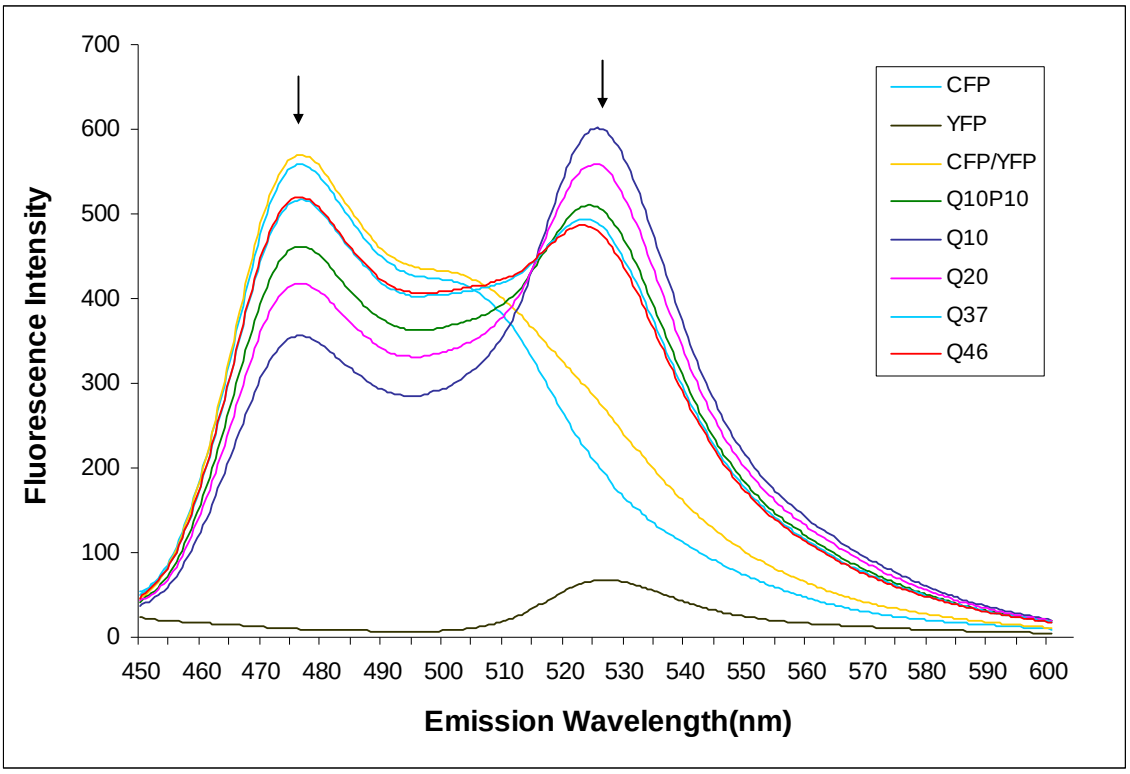

FIGURE 16. CFP-Qn-YFPs yield FRET signal in vitro. His6-tag-CFP-Qn-YFP (300nM) was selectively excited at 434nm, which is optimal for CFP. The scan emission spectra (450 nm-600 nm) are shown. The left arrow indicates the CFP emission peak, the right arrow indicates the YFP emission peak. The emission spectra of CFP and YFP alone, as well as the 1:1 mixture of CFP and YFP, are also included. These control spectra indicate that YFP yields a slight emission signal when directly excited at 434 nm, and FRET does not occur unless CFP and YFP are linked together.

The FRET distances were also calculated based on Eq. 2, assuming R_0 is 50 Å (Table 1). CFP emission intensity with and without YFP at 476 nm (Ex 434 nm) were obtained from duplicate measurements. Q10P10 peptide is about 63 Å in the solution by FRET experiment. It agrees with the X-ray crystallography results, in which Q10P10 bound to Fv is about 52 Å.

We also inserted HD exon1 containing different lengths of polyglutamine (16, 25, 37, and 46) between CFP-YFP fusion proteins. The distance between the N-terminus and C-terminus of HD exon 1 is too far (>100 Å) from each other to yield significant FRET signal (Figure 17).

Table 1. Distance of polyQ tracts determined by FRET

	Linker sequence	**FRET efficiency %**	**R (Å)**
Q10	Q10KL	37.9	54 ± 0.5
Q20	Q20KL	27.0	59 ±0.3
Q10P10	Q10P10KL	18.9	63 ±0.6
Q37	RDPQ37 KL	9.0	73 ±0.5
Q46	RDPQ46 KL	8.5	76 ± 1

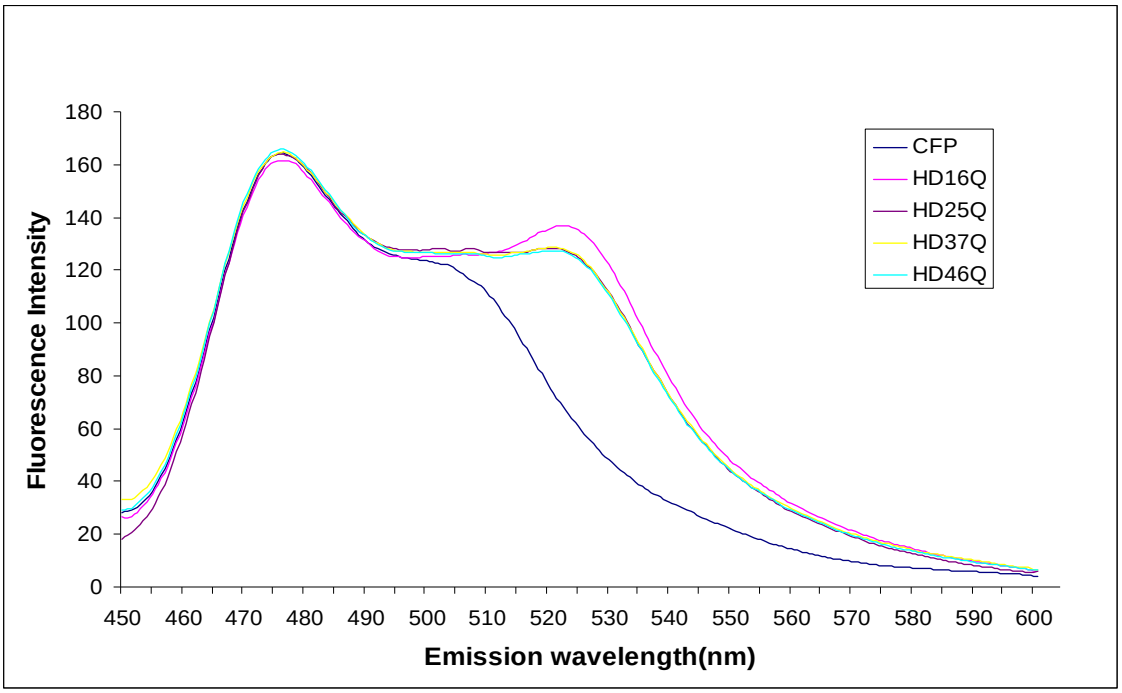

FIGURE 17. CFP-HD exon 1-Qn-YFPs do not yield FRET signal in vitro. The fusion proteins were excited at 434 nm and emission spectra were scanned from 450 nm to 600 nm. The protein concentrations were in 100 nM in Tris-HCl buffer, pH 7.5.

MW1 Fv binds with polyQ tracts

The interaction between MW1 antibody and polyQ was studies with SPR in context of TRX HD-exon1 fusion protein (Bennett et al., 2002). Genes encoding the MW1 V_H and V_L domains were isolated from the MW1 hybridoma. Noncovalent MW1 Fv was refolded from denatured V_H and V_L expressed separately in *E.coli*. Fv and CFP-Qn-YFP were mixed at a 1:1 ratio and analyzed by gel filtration column. Fv and CFP-Qn-YFP alone were applied as control as well. The elution volume of Fv corresponds to an apparent molecular mass equals to 25kDa (Red curve).This is calculated based on the standard curve generated using protein of known molecular mass. The elution volumes of CFP-Qn-YFP (n=10, 20, 37, 46) are 13.95 ml, 13.84 ml, 13.54 ml and 13.21 ml respectively Black curve). After mixing CFP-Q10-YFP and Fv, the mixture shows no peak shift, which suggests no protein complex is formed (Green curve, Fig18A). However, the crystal structure shows that MW1 binds to short peptide epitopes of 10 Gln (Ko et al., 2001; Li et al., 2007). One explanation is that CFP and YFP sequester some of the glutamine residues and less than 10 glutamines are exposed to the binding site of MW1 Fv. MW1 Fv and CFP-Qn-YFPs (when Q≥20) can form a protein complex, which is indicated by a elution volume peak shift to the left after mixing these two proteins (Figure 18 B-D green curve). At the meanwhile Fv peaks diminish correspondingly. These results implicate Fv can bind tightly with CFP-Qn-YFPs and form a stable protein complex when n>20.

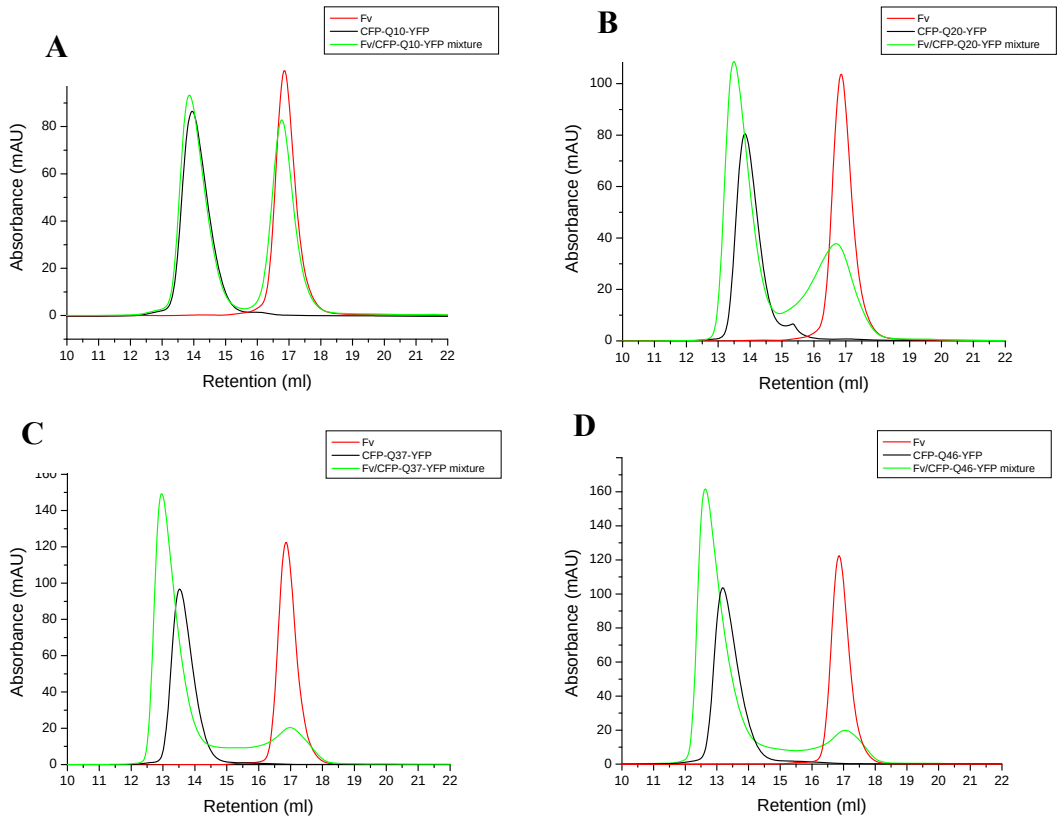

FIGURE 18. Gel permeation chromatography of Fv and CFP-Qn-YFPs. Column: Superdex 200 analytical column (20 ml); sample volume: 100 ul; sample concentration: 50 uM; flow rate: 0.5 ml/min; elution buffer: Tris-HCl, pH 7.5 (A) n=10, The absorbance profile at 280 nm shows two major peaks, 16.84 ml for Fv and 13.95 ml for CFP-Q10-YFP. No peak shifts after combining Fv and CFP-Q10-YFP. (B)(C)(D) n=20,37,46. Fv peak diminishes and the first elution peak shifts to left, which is assumed to be Fv/CFP-Qn-YFP complex (green curve).

CFP-Qn-YFPs tend to aggregate in high concentration

The aggregation of CFP-Qn-YFP fusion protein was monitored by measuring the ratio of Em_{527}/ Em_{476} with Perkin Elmer LS55. Emission spectra were first collected when the concentration of CFP-Qn-YFP equals 200 uM. Then a series of 2 fold dilution

was conducted, and emission spectra were scanned at each diluted concentration (Figure 19). Each spectrum was read three times. The experiments were repeated three times independently.

For all the four fusion protein, FRET efficiencies (implicated by Em $_{527}$/ Em $_{476}$) are apparently higher in higher protein concentration. When the concentrations decrease to about 10uM, the curves become flat. These results suggest that CFP-Qn-YFPs may adopt a different conformation in high concentration to bring the N-terminal CFP and C-terminal YFP in close proximity. When the samples are diluted, the aggregations are reversed. Then the fusion proteins exit as monomer with extended polyglutamine tracts of random coils.

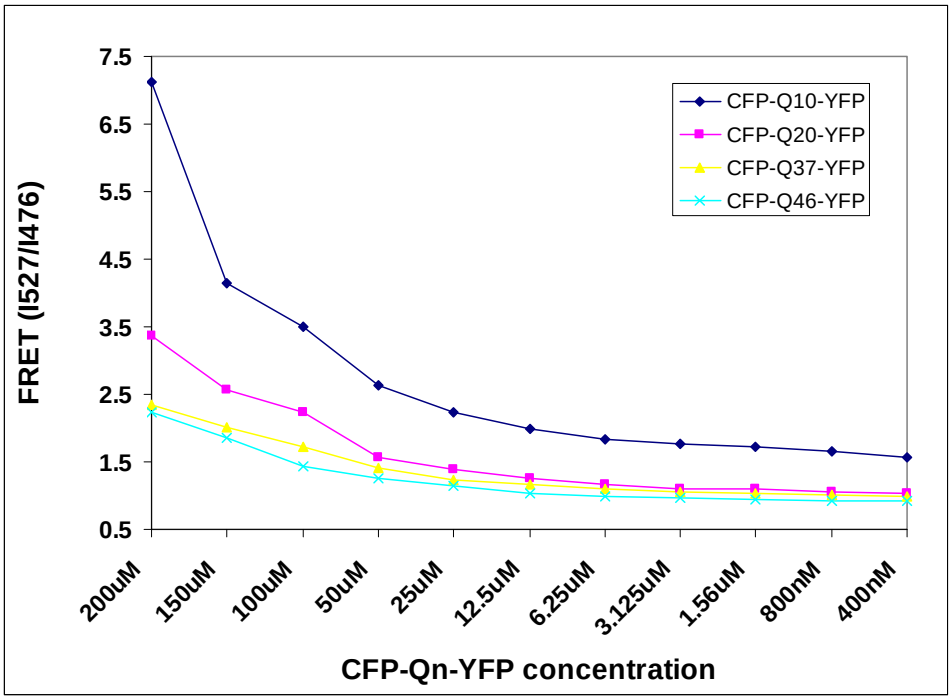

FIGURE 19. Concentration dependence of FRET efficiency. CFP-Qn-YFPs were excited at 434 nm. Emission intensity was measured at 476 nm and at 527 nm respectively. Protein concentrations were diluted consecutively from 200 uM to 400 nM.

MW1 breaks down the aggregated polyQ fusion protein and helps stabilize the protein in a more extended conformation

MW1 Fv binds the polyQ tract with a weak binding affinity (K_d =3 μM). The concentrations of CFP-Qn-YFPs remain constant at 25 μM, and they were titrated with Fv of the increasing concentrations from 25 μM to 50 μM, 75 μM, 100 μM, 125 μM and 150 μM. The ratio of Em_{527}/Em_{476} was obtained as mentioned above. Em_{527}/Em_{476} is 2.18 for CFP-Q10-YFP at 25 μM. After mixing with 25 uM Fv, Em_{527}/Em_{476} reduced to 1.54. This observation implicated that Fv may interact with CFP-Q10-YFP and disrupt its β-sheet structure that exists in high protein concentration. The binding between CFP-Q10-YFP and Fv is too weak to be observed on size exclusion column (Figure 20). CFP-Q10-YFP is totally saturated with Fv if mixing them with a 3:1 ratio. The FRET signal does not decrease further even the ratio increases to 4:1, 5:1 and 6:1. CFP-Q20-YFP shows the similar binding curve as CFP-Q10-YFP. CFP-Q37-YFP and CFP-Q46-YFP show the similar emission spectra. These two proteins are not saturated with Fv until the ratio reaches 5:1. These results suggest that CFP-Q37-YFP and CFP-Q46-YFP have more binding sites for Fv than CFP-Q10-YFP and CFP-Q20-YFP. This finding is consistent with the previous analytical ultracentrifugation experiments. AUC experiments show HD-exon1-46Q can bind multiple copies of MW1 Fv. (See Figure 21) The majority of HD-exon1-46Q bind with one Fv molecule in a 1:1 mixture (Blue curve). HD-exon1-46Q molecule binds two Fv molecules in a 1:2 mixture. HD-exon1-46Q is saturated with Fv in a 1:4 mixture, with four Fv molecules bound to each HD-exon1-46Q.

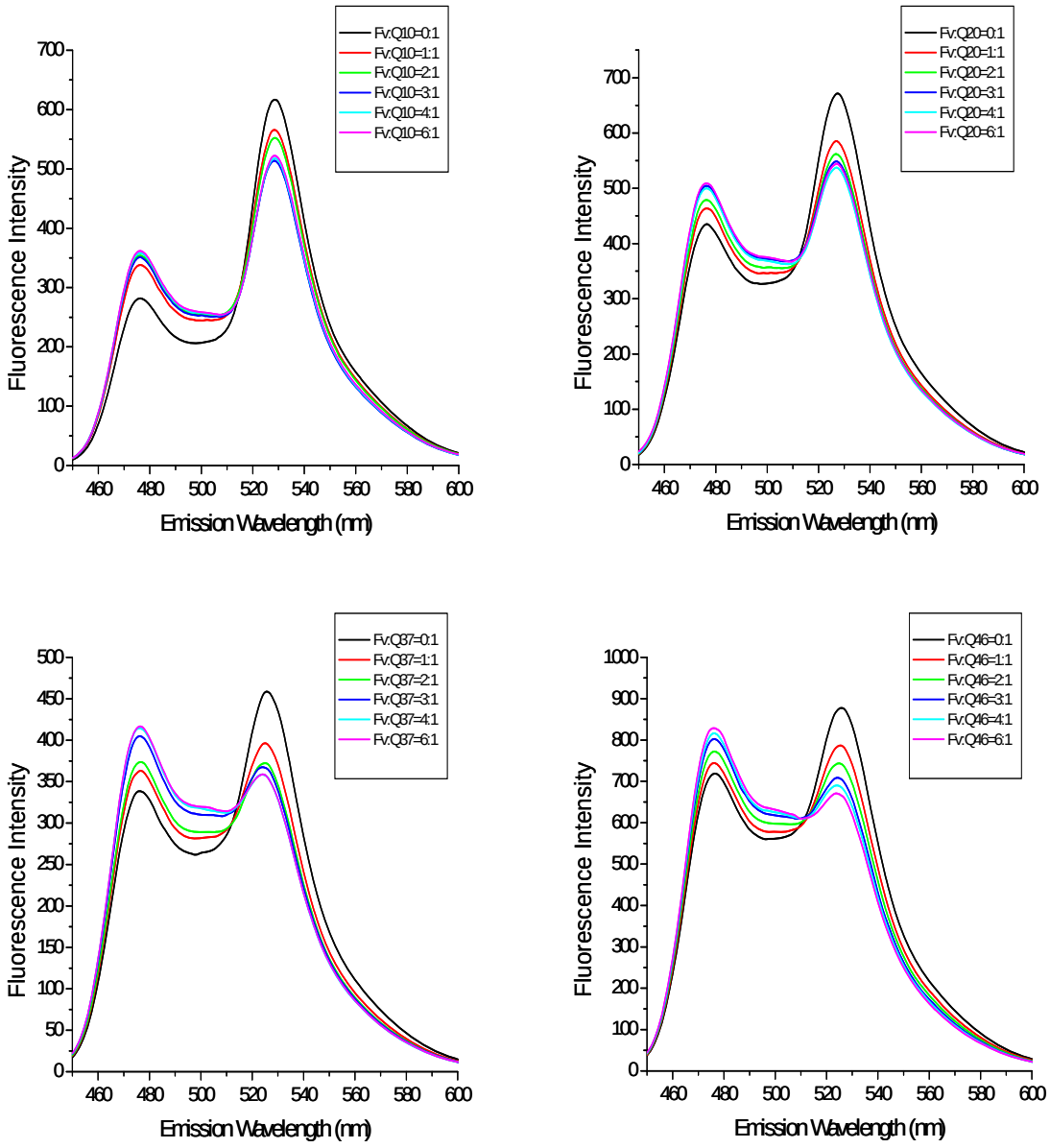

FIGURE 20. FRET spectra of CFP-Qn-YFPs with Fv titration.

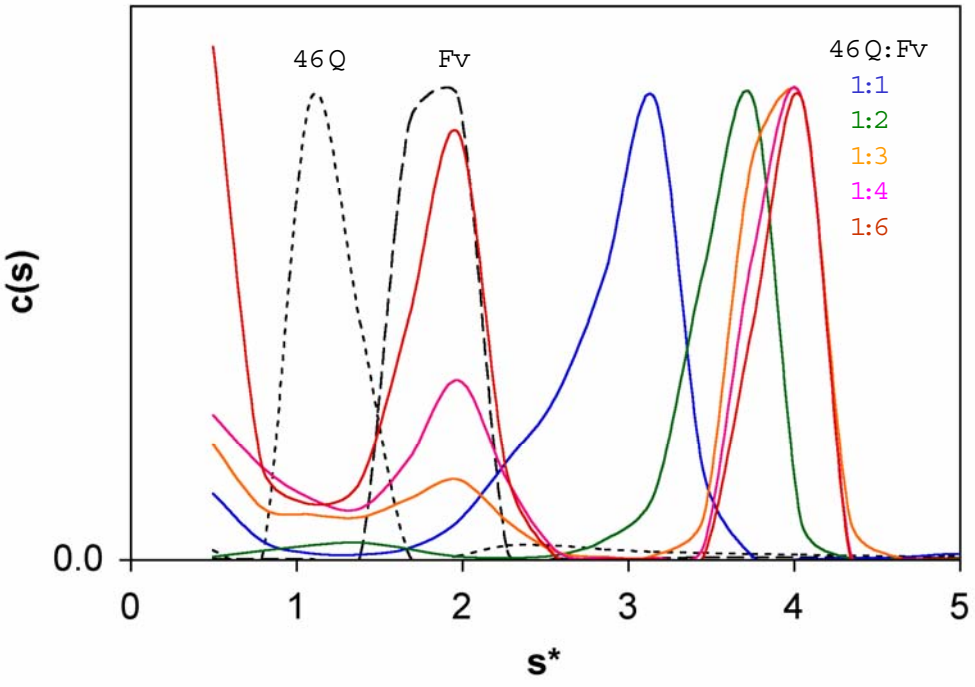

FIGURE 21. AUC experiment of HD-exon 1 and Fv. Plot of the distribution of sedimentation coefficients c(s) versus sedimentation coefficients, s. Sedimentation coefficients are plotted in Svedberg units and calculated from the concentration profiles using SEDFIT.

Crystallization of Fv/Q10P10 complex and structure determination

We expressed SUMO fusion proteins of a peptide containing 10 glutamines and 10 prolines (Q10P10). Fv/Q10P10 complex was generated by cleaving the SUMO tag with SUMO protease and purified with Ni^{2+} affinity column. The Fv-Q10P10 complex was crystallized in 50 mM Tris, 2.0 M $(NH_4)_2SO_4$ at pH 8.5 (Figure 22A). The complex crystallized in $P2_1$ space group with unit cell parameters: a=50.38 Å, b=80.37 Å, c=286.67 Å. We have collected diffraction data for the Fv/Q10P10 complex crystals at

beamline 8.2.2 at ALS. The crystal diffracted to 3.5 Å at ALS using a Quantum 315 CCD detector. The diffraction data were processed with the HKL-2000 package (Otwinowski and Minor, 1997). The structure was determined by molecular replacement using the program MOLREP (CCPN, 1994), with the Fv structure as search model. The molecular model of the peptides was built into the difference map using the program O (Jones and Kjeldgaard, 1997). The structure was refined with CNS (Brünger et al., 1998) to R_{free} of 28.1 and R_{work} of 24.6 (Table 2).

Table 2. Data collection and refinement statistics for MW1 Fv/Q10P10 complex

Data Collection	
Space group	$P2_1$
Cell dimensions	
a, b, c (Å)	50.38, 80.37, 286.67
α, β, γ (º)	90.0, 90.32, 90.0
Resolution (Å)	50-3.15 (3.26-3.15)[a]
Rmege	6.5(22.2)
I/σI	22.9(4.9)
Completeness (%)	90.5(67.2)
Redundancy	3.0(3.0)
Refinement	
Resolution (Å)	50-3.15
No. Reflections	33904
R_{work}/R_{free}	24.6/28.1
No. atoms	
Protein	10890
Peptide	451
R.m.s deviations	
Bond lengths (Å)	0.014
Bond angles (º)	1.90
[a]Values in parentheses are for highest-resolution shell.	

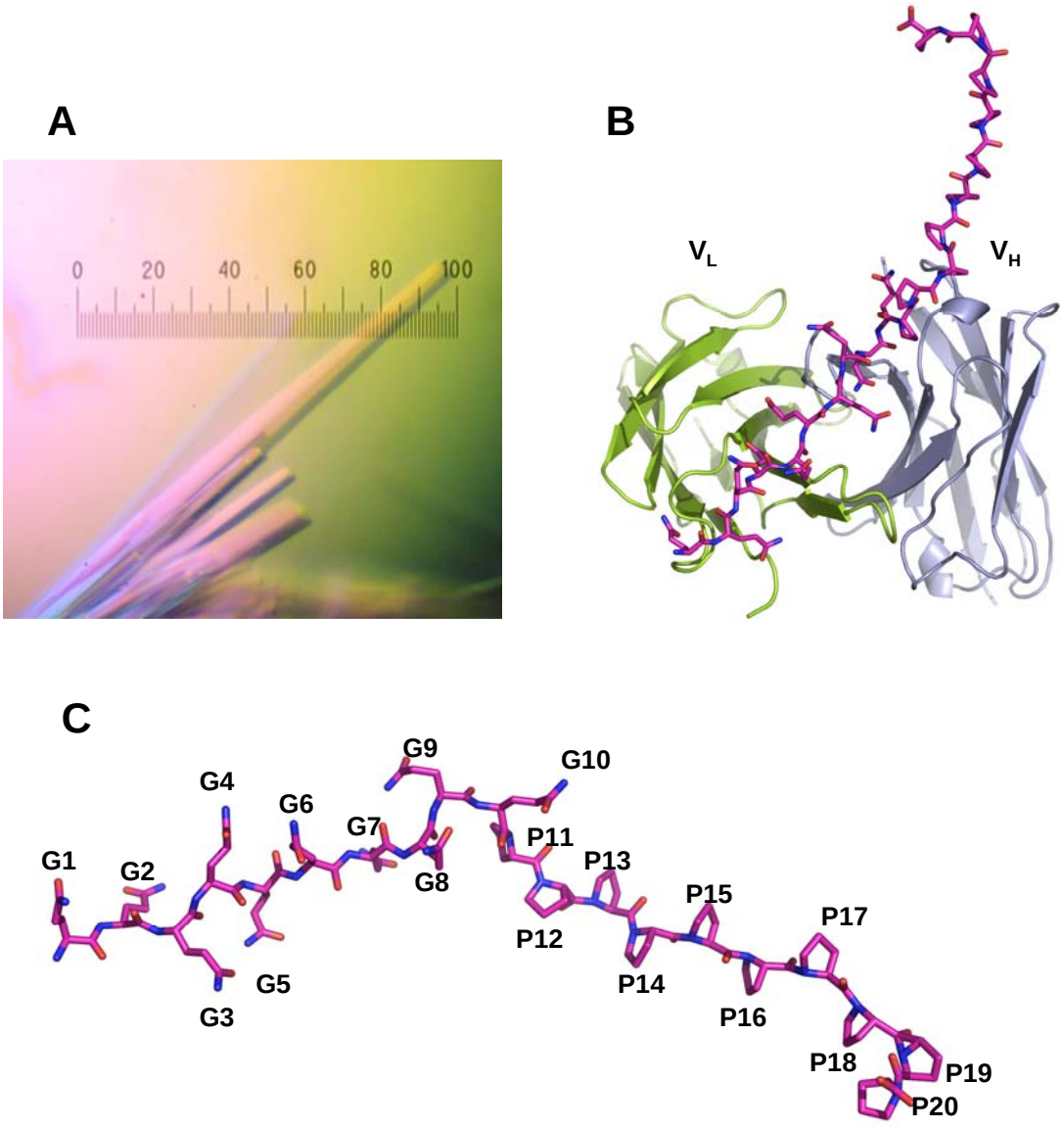

FIGURE 22. Structure of Q10P10 peptide bound to MW1 Fv. (A) Crystals of MW1 Fv/ Q10P10. (Each 10 division of the scale is 66um.) (B)Structure of Fv/Q10P10 complex, V_L chain (green) and V_H chain (light blue) are shown in ribbon diagram, while Q10P10 peptide is shown in stick diagram. (C) Structure of Q10P10 peptide.

The Q10P10 peptide adopts an extended structure about 52 Å long and lies in the pre-existing diagonal groove of Fv. The overall structure of the Q10 region shows the same features as Q10 peptide in Fv/Q10 complex (Li et al., 2007). Residues Gln 2, 4, 8 and 10 have the main chain dihedral angels of polyproline II helix. No hydrogen bonds were found between a glutamine side chain and the backbone carbonyl oxygen of the following residue, which is a characteristic of polyproline II helix. Gln5-7 form a short β-strand to interrupt the PPII helical structure. The P10 region does not bind with Fv molecule and sticks out to form a typical polyproline helical structure. The extended structure of polyproline is stabilized by crystal packing contact. The polyproline region does not seem to affect polyQ conformation as expected (Figure 22B, C).

CHAPTER III

MOLECULAR MECHANISM OF TLR SIGNALING

Objective

Although the previous research study has given us a framework of proteins involved in TLRs signaling, the structure basis of protein-protein interaction is poorly understood. My primary goal is to study the molecular mechanism of TLR signaling using combination of structural and biochemical approaches.

Specific aim 1: Elucidate the mechanism of MyD88 recruitment to TLRs

MyD88 mediate TLRs signaling through homotypic interaction with TLR TIR domain. TLR TIR domains have average 30% sequence identity and the conserved core structure, but their surface structures have variance. There are two possible explanations for how MyD88 acts as a universal adaptor: 1) MyD88 interacts with TLRs by a conserved motif shared between different TLRs. 2) MyD88 interacts with TLRs with different interfaces. To investigate this problem, the most direct way is to obtain MyD88 TIR and TLRs TIR complex and compare the structure to find out the answer.

Specific aim 2: Indentify residues involved in MyD88 death domain and IRAK4 death domain interaction

There are two steps for forming the platform. 1) MyD88 oligomerization 2) MyD88 recruits IRAK4/IRAK1 via DD/DD interaction. We are interested in residues involved in both MyD88 oligomerization and DD/DD interaction motif.

Specific aim 3: Investigate the mechanism of IRAK1 ubiquitination by Pellino1

We previously determined the structure of Pellino1 and found its unique two RING-finger motif. A crystal complex of Pellino1/Ubc13/Uev1a or Pellino1/UbcH3 will help us to understand the different mechanism, by which Pellino1 catalyzes polyubiquitin chain linkage.

Experimental Procedures

Construction of expression vectors

MyD88, Pellino1, Ubc13 and Uev1a cDNA were purchased from Open Biosystem. Pellino1 baculovirus was generated by Xiaojun Li. pGEX-IRAK4DD and pBAC-TLR5-TIR were generated by Dr. Pingwei Li. DNA primers were ordered from Integrated DNA Technologies (Table 3). Primers were dissolved in ddH_2O to make a final concentration of 1 mg/ml. MyD88 DD (19-136) was inserted between NdeI and SalI site of pET28. Pellino1 was inserted between BamHI site and XhoI site of pBAC. Ubc13 and Uev1a were inserted between NdeI and XhoI site of pET28. Plasmids were transformed into DH5α cell. All the expression vectors were confirmed by DNA sequencing. (LPGT, Texas A&M)

Table 3. Oligonucleotides used for construction of expression vectors

Expression vectors	Sense primers	Anti-sense primers
pET28 MyD88 DD (19-136)	5' tatatatacatatgtcccttcccctggctgctctc 3'	5' tatatagtcgacttagctgtctacagcggccacctg 3'
pET28 Ubc 13 (1-152)	5' tatatatacatatggccgggctgccccgcagg 3'	5' tatatagtcgacttaaataataatcatggcatatag 3'
pET28 Uev1a (8-147)	5' tatatatacatatgggagtaaaagtccctcgc 3'	5' tatatagtcgacttaattgctgtaacactgtcc 3'
pET28 UbcH3 (7-184)	5' tatatatacatatgcccagctcgcagcag 3'	5' tatatagtcgactcagggcaccttcacgccgtc 3'
pBAC MyD88	5' tatatagaattcatggctgcaggaggtcccggc 3'	5' tatatactcgaggggcagggacaaggccttggcaag 3'
pBAC MyD88 TIR	5' tatatagaattcatgcctgagcgtttcgatgccttc 3'	5' tatatactcgaggggcagggacaaggccttggcaag 3'
pBAC TLR3 TIR (748-904)	5' tatatagaattcatggacagacagacagaacagtttg 3'	5' tatatactcgagatgtacagagtttttggatcc 3'
pBAC TLR4 TIR	5' tatatagaattcatgggtagaggtgaaaacatc 3'	5' tatatactcgaggatagatgttgcttcctgcc 3'
pBAC TLR9 TIR (862-1032)	5' tatatagaattcatggggcgagatgaggatgccctg 3'	5' tatatactcgagttcggccgtgggtccctggcag 3'
pBAC TIRAP TIR (79-221)	5' tatataggattcatgagtagtcgctggagcaaagac 3'	5' tatatactcgagactgagtgtctgcagataacgc 3'
pBAC TRIF TIR (380-600)	5' tatatagaattcatgtccacatcccctgttttggac 3'	5' tatatactcgagccccagtgacaagttcttccc 3'

Site directed mutagenesis

Primers were dissolved with ddH_2O to a final concentration of 125 ng/ul (Table 4). Mutagenesis PCR reaction was mixed as follows: 50 ng DNA template, 1ul each primers, 5 ul of 10x reaction buffer, 1 ul of dNTP mixture, 1 ul of Pfu Ultra DNA polymerase (2.5 U/ul), ddH_2O to a final volume of 50 ul. The thermal cycles are as follows: preheating to 95°C for 2 min, then 16 cycles of denaturing at 95°C for 30 sec, annealing at 55°C for 30 sec and elongation at 68 °C for 1 min, followed by cooling at

4°C. 1 ul of Dpn I restriction enzyme was added directly to PCR products and incubated for 2 hrs at 37°C to digest the parental DNA. 1 ul of Dpn I-treated DNA was added to 60 ul XL1-Blue supercompetent cells, heat shock for 45 sec at 42°C and then place the reactions on ice for 2 mins. 0.5 ml of SOC media was added to the transformation reactions at 37°C for 1 hour with shaking at 250 rpm. 100 ul of cells were spread on agar plate and incubated overnight at 37°C. Colonies were picked and plasmids were prepared by Miniprep and sent for sequencing.

Table 4. Primers used for site directed mutagenesis

mutation	sense primers	antisense primers
R40S	5’CTGTTCTTGAACGTGAGCACACAGGTGGCG3’	5'CGCCACCTGTGTGCTCACGTTCAAGAACAG3'
R62S	5'GTGTCTCCAGTTGGCTGATCTCCAAGTACTC3'	5'GAGTACTTGGAGATCAGCCAACTGGAGACAC3'
R81S	5'GACGCCTGGCAGGGAAGCCCTGGCGCCTCTG3'	5'CAGAGGCGCCAGGGCTTCCCTGCCAGGCGTC3'
R88S	5'GCCTCTGTAGGCAGCCTGCTCGAGCTGCTTAC3'	5'GTAAGCAGCTCGAGCAGGCTGCCTACAGAGGC3'
R98S	5'CTTACCAAGCTGGGCAGCGACGACGTGCTGC3'	5'GCAGCACGTCGTCGCTGCCCAGCTTGGTAAG3'
E52Q,R62S	5'CTCAAAGTCCATCTCCTGCGCCAGCGCGGTC3'	5'GACCGCGCTGGCGCAGGAGATGGACTTTGAG3'
E53Q,R62S	5'CGCGCTGGCGGAGCAGATGGACTTTGAGATC3'	5'GATCTCAAAGTCCATCTGCTCCGCCAGCGCG3'
D55N,R62S	5'CTGGCGGAGGAGATGAACTTTGAGTACTTGGAG3'	5'CTCCAAGTACTCAAAGTTCATCTCCTCCGCCAG3'
E57Q,R62S	5'GAGGAGATGGACTTTCAGTACTTGGAGATCAGC3'	5'GCTGATCTCCAAGTACTGAAAGTCCATCTCCTC3'
E60Q,R62S	5'GACTTTGAGTACTTGCAGATCAGCCAACTGGAG3'	5'CTCCAGTTGGCTGATCTGCAAGTACTCAAAGTC3'
R62S,E65Q	5'GAGATCAGCCAACTGCAGACACAAGCGGACC3'	5'GGTCCGCTTGTGTCTGCAGTTGGCTGATCTC3'
R62S,D69N	5'CTGGAGACACAAGCGAACCCCACTGGCAGG3'	5'CCTGCCAGTGGGGTTCGCTTGTGTCTCCAG3'

Sf9 cell culture and transfection

pBAC vectors were heat shock in water bath of 65 °C for 15 min. 4 x 10^6 Sf9 cells in 5 ml volume were seeded in one T25 flask and placed in 27 °C incubator for 30 min for cell attachment. Transfection mixture were prepared as followings: 200 ul Grace’s media , 2 ul BaculoGold ^{TM} DNA (BD Pharmingen), 5 ul Insect GeneJuice Transfection Reagent and 20 ug pBAC vector. Old Media were taken out and replaced with 4 ml Grace’s media after cell attachment to T25 flask. Transfection mixture was added to Sf9 cell and mixed well by rocking the flask back and forward. Sf9 cells were incubated at 27°C for 14-16 hrs. Grace’s media were replaced with 4 ml fresh HyQ-SFX media, and incubated for 4-5 days. Cell culture was centrifuged at 4000 rpm for 5 min. Supernatant was stored with 0.5 ml FBS as P1 virus.

Baculovirus amplification

10^7 Sf9 cells were seeded in T75 tissue culture flask in a total volume of 14 ml HyQ-SFX media. 2 ml P1 virus was added and placed in 27°C incubator for 5 days. Cell media were harvested and saved as P2 virus with 1.5 ml FBS supplement. 2.5 x 10^6/ml x 500 ml Sf9 cells were seeded in each 2L flask. 8-10 ml P2 virus were added and stirred at 100-120 rpm in 27°C incubator for 4 days. Supernatant was collected by spinning at 4000 rpm for 5 min and stored as P3 virus with 10% FBS.

Protein large scale expression and protein purification

2.5x 10^6/ml x 500 ml Sf9 cells were seeded in each 2 L flask. 40-60 ml of P3 virus was added and stirred at 100-120 rpm in 27 °C incubator. Cells were harvested after 2-3 days at 2000 rpm for 5 min. Cell pellets were dissolved in 50 ml lysis buffer (10% NP40, 0.2 M Tris-HCl, 0.15 M NaCl, pH 8.0). Cell lysate was gently mixed for 1 hr at 4°C and spinned down at 16,000 rpm for 30 min. Supernatant was added with 5 ml Ni-NTA beads and mixed at 4°C for 2 hr. Ni-NTA beads were spinned down at 4000 rpm for 1 min and washed with wash buffer for 3 times (10 mM imidazole，20 mM Tirs-HCl, 150 mM NaCl, pH 8.0). Protein was eluted with 10 ml elution buffer (0.25 M imidazole, 20 mM Tris-HCl, 150 mM NaCl, pH 8.0). 5 mM DTT and protease inhibitor was added to the eluted protein and stored at 4°C.

Preparation of ^{15}N MyD88DD (E52QR62S) for HSQC

BL21 cells containing pET28 MyD88DD (E52QR62S) was inoculated to 2 x 1L Minimal Media (Tables 5, 6, 7). Proteins were expressed and purified as described above. Protein solution (pH 6.5) is added to Shigemi NMR tube by pipetting slowly with a standard pipetter. If the sample becomes trapped by an air bubble before it reaches the bottom, stop adding sample and gently shake the tube to use centrifugal force to get the sample to the bottom. The plunger was inserted until it reaches the top of the sample. To remove air bubbles, rest the bottom of the tube on a table or other firm surface and

gently tap the plunger to force liquid and air around the plug. The top of the tube was sealed with parafilm and sent to Biomolecular NMR Lab, Texas A&M.

Table 5. Minimal media

	Amount (ml)	Notes
10x Minimal Salts	100	
Trace Elements	5	
$MgCl_2$	5	1.0 M (autoclaved)
Thiamine	2	20 mg/ml, sterile filtered
Kanamycin	2	100 mg/ml, sterile filtered
Glucose	40	20%, autoclaved
H_2O	850	

Table 6. 10x Minimal salts

Compound	Amount (g/100 ml)	Notes
KH_2PO_4	13.0	
$K_2HPO_4 \cdot 3H_2O$	13.1 (10.0 g anhydrous)	Adjust to pH 7.2–7.4 with KOH. pH should be about 6.7 before adjustment
Na_2HPO_4	9.0	
K_2SO_4	2.4	
$^{15}NH_4Cl$	1.1	Autoclave

Table 7. Trace elements

Compound	Amount (g/100 ml)	Instructions
$EDTA\text{-}Na_2$	0.50	
$CaCl_2 \cdot 2H_2O$	0.60	Add the EDTA to a fraction of the water. Add each ingredient separately with stirring and wait several minutes. Add the rest of the water, wrap the container in foil and stir overnight. The color should turn from green to gold.
$FeSO_4 \cdot 7H_2O$	0.60	
$MnCl_2 \cdot 4H_2O$	0.115	
$CoCl_2 \cdot 6H_2O$	0.08	
$ZnSO_4 \cdot 7H_2O$	0.07	
$CuCl_2 \cdot 2H_2O$	0.03	
H_3BO_3	0.002	Sterile filter
$(NH_4)_6Mo_7O_{24} \cdot 4H_2O$	0.025	

GST-tag pull down

GST-IRAK4DD fusion protein and MyD88DD were immobilized on Glutathione Sepharose 4 Fast Flow (GE Healthcare, AB) by incubating the purified GST-IRAK4DD with beads at 4 °C nutation for 1 hr. The beads were washed 3 times with PBS buffer (140 mM NaCl, 2.7 mM KCl, 10 mM Na_2HPO_4, 1.8 mM KH_2PO_4, pH 7.3) by centrifugation at 500g for 5 min. The bound protein was eluted by adding 0.5 ml 50 mM Tris-HCl, 10 mM reduced glutathione, pH 8.0 per 1 ml slurry of Glutathione Sepharose 4 Fast Flow.

Polyubiquitination assay

A mixture of 0.1 uM E1, 1 uM Ubc13-Uev1a, 1 uM Pellino1, 0.1 mM ubiquitin, 5 mM $MgCl_2$, 2 mM ATP and with or without 1 uM GST-IRAK1 was incubated for 1 hr at 37°C in a total volume of 50 ul Tris-HCl buffer, pH 7.5. The reaction was terminated by the addition of SDS and resolved by SDS-PAGE.

Results

Protein expression of TIR domains

Our study on TIR-TIR domain interaction is hindered by the poor solubility and stability of TIR domains. The expression of TIR domains of TLR1, TLR2, TLR3, TLR4, TLR5 and TLR9 were tried in both *E.coli* and Sf9 cells. Sf9 cells can yield a small amount of TLR4-TIR (<1 mg/L) (Figure 23). After Ni-NTA beads purification, the purified TIR domain proteins were shown on SDS-PAGE. When the TIR domain proteins were loaded on the size exclusion column, the elution profile did not show a sharp single elution peak. It is because these TIR domain proteins tend to aggregate during the protein purification process. TIR domain of the three adapter proteins: MyD88, TIRAP and TRIF were also expressed in both *E.coli* and Sf9 cells. The soluble proteins of TIRAP-TIR and MyD88 (E52QR62S) can be produced in pBAC vector in Sf9 cells (Figure 24). These proteins are stable only in low concentration (<2mg/ml). Alternative strategies like co-transformation, co-infection or adding GST-tag were applied to improve the protein stability and solubility, but little progress was achieved.

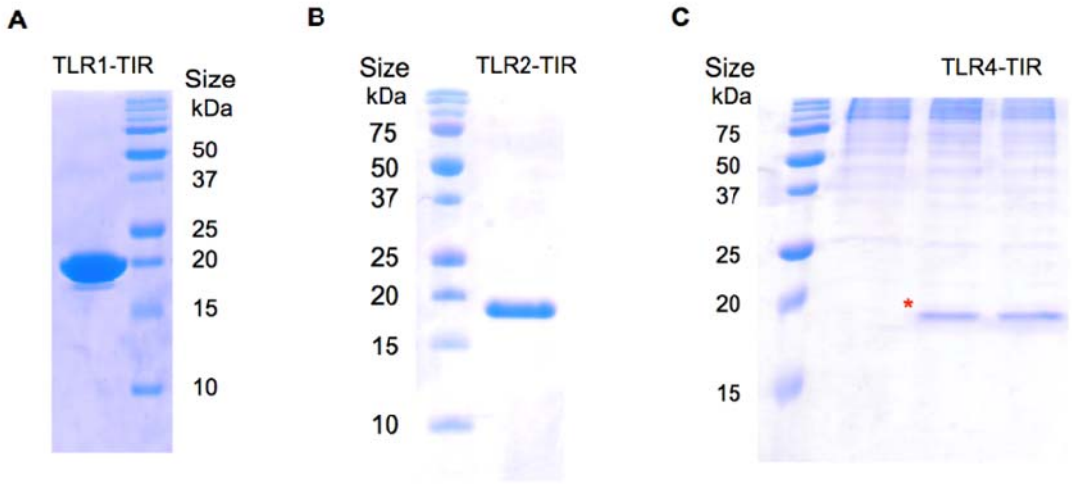

FIGURE 23. SDS-PAGE of TLR1 (A), TLR2 (B), and TLR4 (C) TIR domains.

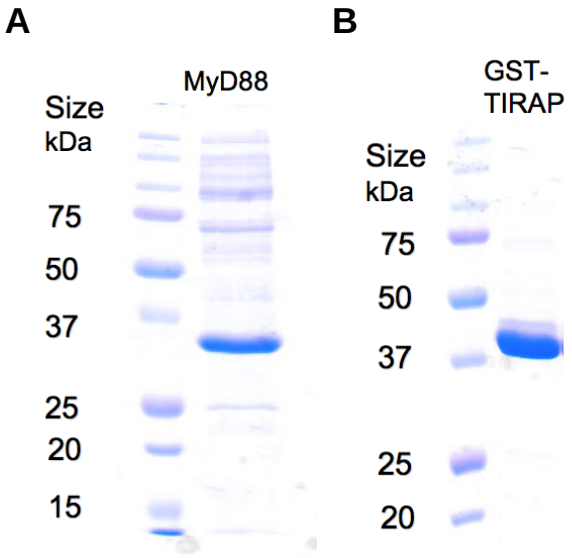

FIGURE 24. SDS-PAGE of full length human MyD88 (A) and GST-TIRAP TIR domain (B).

Protein expression of IRAK4DD and MyD88DD in *E.coli*

IRAK4DD was inserted to pGEX vector with GST-tag at the N-terminal as described (Lasker et al., 2005). MyD88DD was inserted into pET28 vector with N-terminal His-tag. Both protein express vectors were transformed into BL21 and induced at 15°C for 14-16 hours. Both proteins were purified with either GST-tag or His-tag affinity chromatography, followed by size exclusion chromatography. Both proteins have a decent protein yield (~20 mg/L) (Figure 25). GST-tag and His-tag were cleaved off with thrombin and remove by size exclusion column. IRAK4DD is stable in Tris-HCl buffer, pH 7.5, but MyD88DD tends to oligomerize under the same condition. Monodispersed MyD88 death domain is needed for the study of IRAK4 death domain and MyD88 death domain interaction.

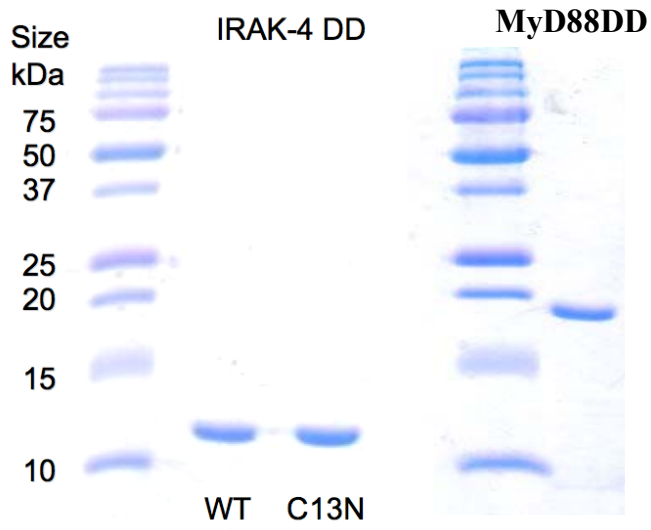

FIGURE 25. SDS-PAGE of IRAK4 death domain and MyD88 death domain.

E52QR62S disrupts MyD88DD oligomerization

MyD88DD oligomerization cannot be disrupted by extreme pH or high salt concentration. MyD88DD sequence alignment and the secondary structure prediction were conducted. Eight residues were randomly selected on the conserved charge regions for site mutagenesis to neutralize the positive charge (Figure 26A). These mutants were expressed, purified and analyzed with size exclusion column. A crucial mutant, R62S for MyD88DD oligomerization was identified. The mutation of Arg62 to serine on helix 2 disrupts MyD88DD oligomerization and stabilizes it in dimeric form. Other mutations had little effect on MyD88DD oligomerization (Figure 26B).

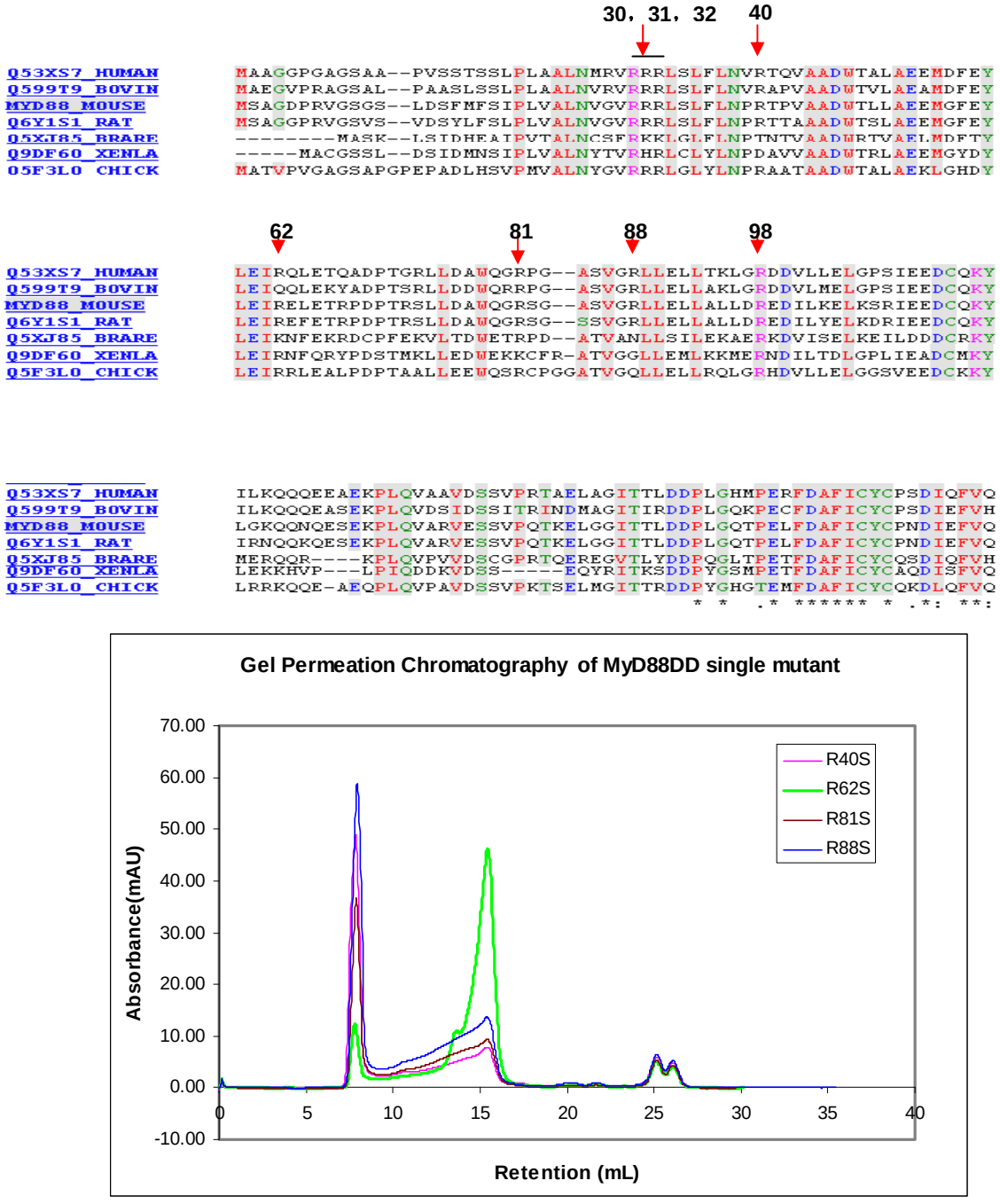

FIGURE 26. Site mutagenesis of MyD88 death domain. (A) Sequence alignment of MyD88. The mutation sites are indicated by red arrow. (B) Gel permeation chromatography of four soluble MyD88 death domain mutants. R62S is represented by green curve.

For crystallization, protein concentration must reach a critical value (usually > 10 mg/ml). Although the single R62S mutant is stable in a low concentration (~ 2mg), it aggregates during the concentration process. Thus, seven double-mutants on helix 2 were screened and compared on the gel permeation chromatography. E52QR62S has the sharpest elution peak among all (Figure 27). This double-mutant MyD88DD is monodispersed in high concentration (~15 mg/ml). Therefore, it could be a good candidate for protein crystallization and NMR experiments.

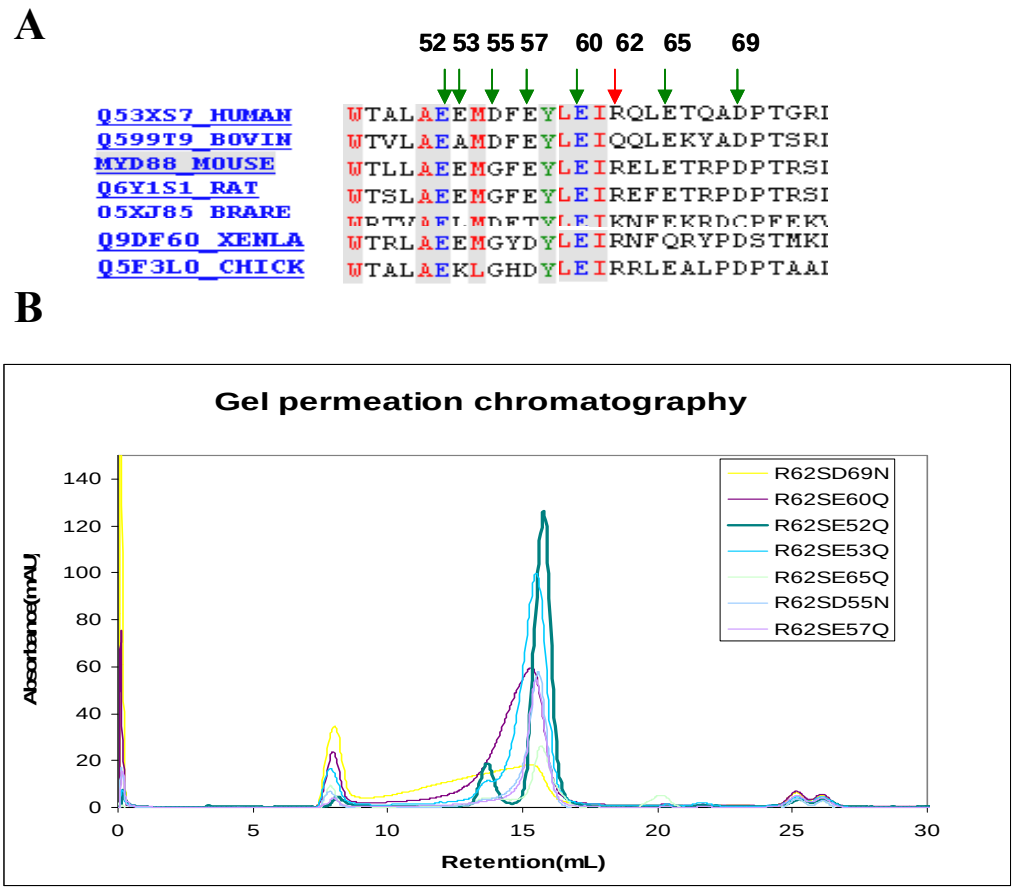

FIGURE 27. Site mutagenesis of helix 2 in MyD88 death domain. (A) Sequence alignment of MyD88 helix 2. The mutation sites of negative charge are indicated by green arrow. (B) Gel permeation chromatography of seven soluble MyD88DD double-mutants. E52QR62S is represented by green curve.

GST pull down of MyD88DD (E52QR62S) and IRAK4DD

MyD88DD can interact with IRAK4DD and activate the down stream of TLR signal pathway. To make sure that the MyD88DD (E52QR62S) retains the function as the wild type MyD88, GST-pull down experiments were conducted to test the binding between MyD88DD (E52QR62S) and IRAK4DD. GST-IRAK4DD and MyD88DD (E52QR62S) were expressed in *E.coli* as describe above. GST-IRAK4DD and MyD88DD (E52QR62S) were mixed at a 1:1 molar ratio and incubated with Glutathione Sepharose beads for 2 hours. The beads were washed with PBS buffer for 3 times and eluted with 50 mM reduced glutathione. MyD88DD (E52QR62S) can bind with IRAK4DD and comes out in the elution buffer with GST-IRAK4DD (Figure 28). The same procedures were carried out with only GST-IRAK4DD or MyD88DD as control.

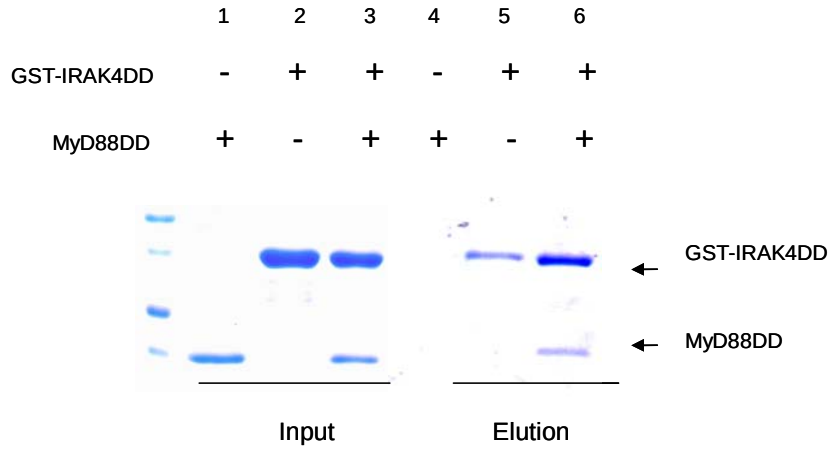

FIGURE 28. GST pull down of IRAK4 death domain and MyD88 death domain.

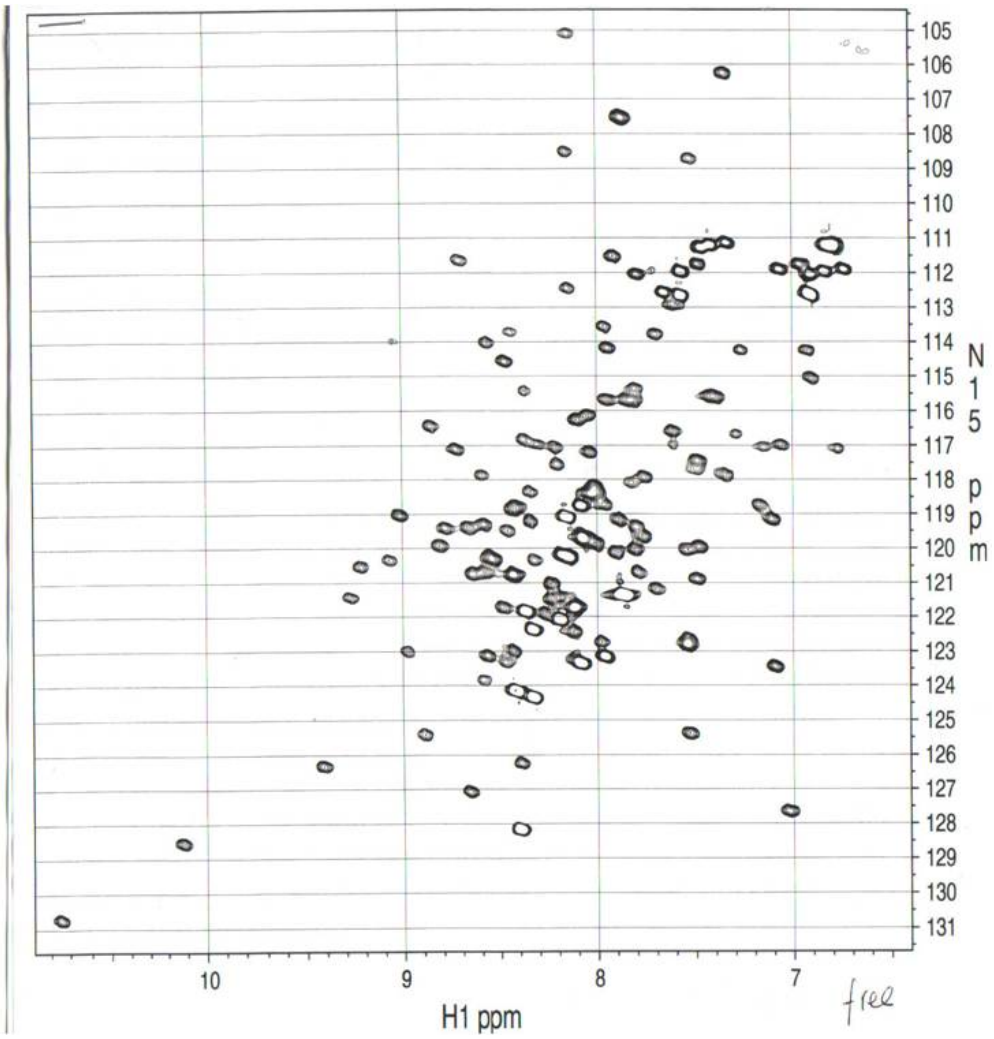

FIGURE 29. 2D ^{1}H-^{15}N HSQC of MyD88DD (E52QR62S). (1 mM in Tris-HCl buffer, pH 6.5) The experiments were carried out by Biomolecular NMR Lab, Texas A&M.

HSQC of MyD88DD (E52QR62S)

The crystallization trial of MyD88DD (E52QR62S) was carried out with 300 crystallization conditions, but none of them yielded a crystal. NMR spectroscopy was applied to solve the structure of this protein as an alternative method, since MyD88DD (E52QR62S) is within the range of NMR study (~17KDa). ^{15}N HSQC experiment is probably the most frequently recorded experiment in protein NMR spectroscopy. Each residue of the protein (except proline) has an amide proton attached to a nitrogen in the peptide bond. Each N-H group gives an individual cross peak because of the different environments. If the protein is folded, the peaks are usually well dispersed, and most of the individual peaks can be distinguished. The number of peaks in the spectrum should match the number of residues in the protein plus the sidechains with nitrogen-bound protons, like argine and lysine. H^1 -^{15}N cross peak are well disperse and each one represent on N-H group (Figure 29). Thearetically there are 131 N-H groups in the protein. On the HSQC spectrum, there are about 120 individual peaks. It sounds a good alternative method to solve the structure by NMR spectroscopy based on this preliminary HSQC spectrum.

Expression of Pellino1 and Ubc13/Uev1a

Ubc13 and Uev1a were expressed in pET28 vector and purified as described (Zhang et al., 2005). Pellino1 was inserted in pBAC vector and expressed in Sf9 insect cells. All three proteins were first purified by His-tag affinity column and followed by Superdex sizing column. The purified proteins were loaded on SDS-PAGE to check purity. A clear single band of SDS-PAGE (Figure 30) and a single peak on gel permeation chromatography (data not shown) indicate that the proteins are pure enough for protein crystallography.

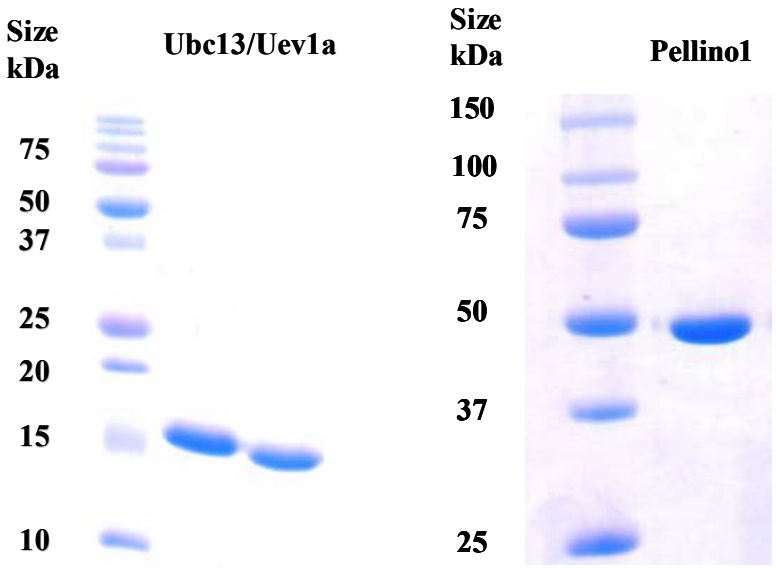

FIGURE 30. SDS-PAGE of Pellino1, Ubc13 and Uev1a.

Pellino1 (E3) induces the formation of pUb chains in the presence of Ubc13/Uev1a (E2)

The human genome is thought to encode one E1 enzyme, 50 E2 conjugating complexes and over 500 ubiquitin E3 ligases. It is like a pyramid structure. Each E2 conjugating complex must operate with 10-20 E3 ligases. E3 ligases are responsible for the substrate specificity. In the previous study, Pellino1 was able to catalyze the formation of polyubiquitin in conjunction with five E2 complexes in vitro (Ordureau A et al., 2008). In the presence of Ubc13/Uev1a and active IRAK1, Pellino1 induces the formation of pUb chains (Figure 31, lane 4). A catalytical inactive mutant of IRAK1 greatly decrease its ligase function (Figure 31, lane 3). Taking together, wild type IRAK1 phosphorylates Pellino1 and enhances its E3 ligase activity. The main purpose of this assay is to make sure that the proteins used for crystallization are properly folded and retain its function.

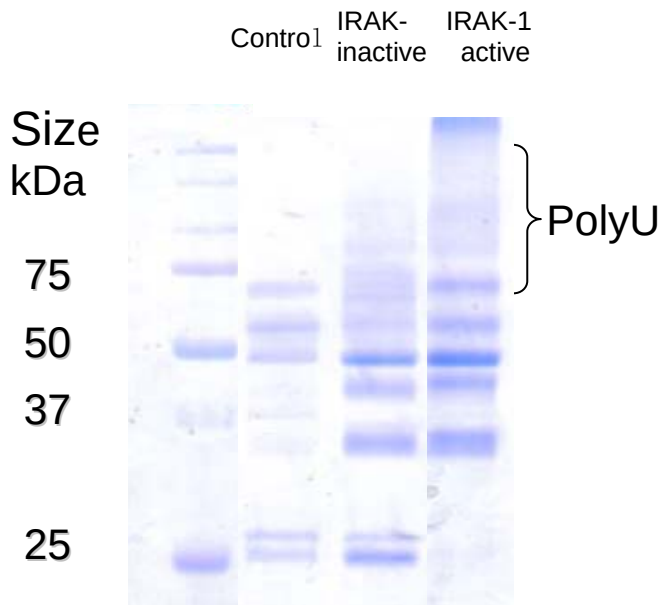

FIGURE 31. IRAK1 phosphorylates Pellino1 and enhances its E3 ligase activity. A mixture of 0.1 uM E1, 2 uM Ubc13-Uev1a, 5 uM Pellino1, 0.5 mM ubiquitin, 5 mM $MgCl_2$, 1 uM IRAK1 (inactive or active) and without ATP (lane 1) or with ATP (lane 2,3) in 50 mM Tris-HCl buffer pH 7.5 was incubated for 2 hours at 37 °C in a total volume of 50 ul. The reaction was stopped by the addition of SDS and the samples were loaded on SDS-PAGE and visualized by Coomassie Blue.

Co-crystallization of Pellino1 and Ubc13/Uev1a

Ubc13 and Uev1a were first mixed at a 1:1 ratio and the protein complex was isolated from free Ubc13 and Uev1a with Superdex 200 column. Then Ubc13/Uev1a complex was mixed with Pellino1 at 1:1 molar ratio. Since the binding between Ubc13/Uev1a and Pellino1 was weak, the complex of three proteins was not formed on Superdex 200 column. The mixture of three proteins was concentrated to 10 mg/ml. Protein crystallization was set up by hanging drop method with 200 conditions from Crystal Screen kit and Index kit (Hampton Research, CA). Needle clusters of protein crystal were found in the following two conditions: 0.1 M $Na(CH_3)_2AsO_2 \cdot 3H_2O$，1.4 M $CH_3COONa \cdot 3H_2O$, pH 6.5 and 1.8 M NaH_2PO_4, K_2HPO_4, pH 5.0 (Figure 32). These

conditions were optimized to generate single crystals for data collection. However, the difficulties in crystallization protein complex prevent us from fully achieving the above goals. However, the progress describe in the thesis provide a foundation for future work.

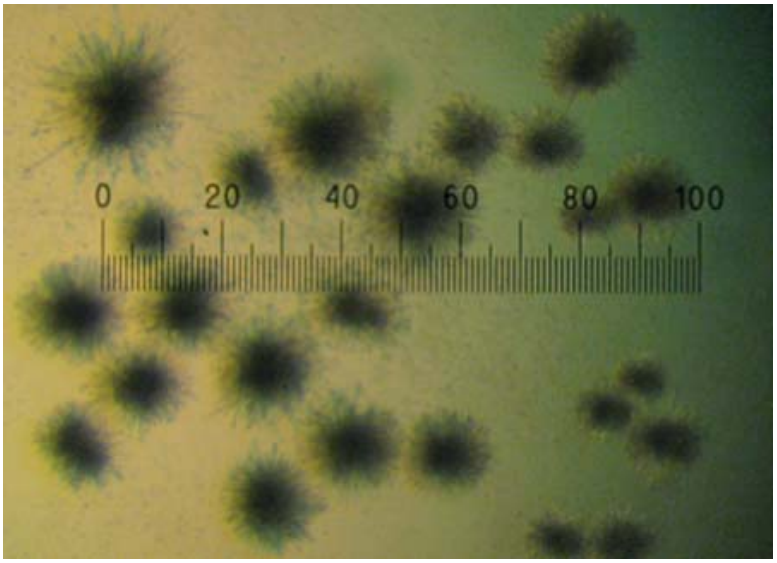

FIGURE 32. Crystals of Pellino1/Ubc13/Uev1a complex. (Each 10 divisions of the scale corresponds to 66 μm.)

CHAPTER IV

CONCLUSIONS

Polyglutamine Conformation

In the first part of the thesis, we studied the polyglutamine conformation in pre-aggregation stage using fluorescence resonance energy transfer. We constructed a series of CFP-Qn-YFP fusion proteins. This simple system enabled us to assess conformational changes, oligomerization, and fibril formation. Our FRET data reveal that both the normal and pathologic polyglutamine adopt the same random coil extended structure in low concentration (300 nM). There was no global conformational change for polyQ tracts longer than 36 residues. FRET efficiency was determined by the number of glutamine residues in polyQ tract. Our experimental results also showed that FRET efficiency is concentration dependent. When concentration increases, FRET efficiency increased accordingly. This finding suggests that polyQ may adopt a β-strand structure to bring CFP and YFP in close proximity. We proposed a "tug of war" model to combine the concentration dependent phenomenon and the linear model (Bennett, 2002): PolyQ peptide exits in a tug of war between two conformations: a random coil and a β-sheet. 1) Irrespective of peptide length, polyQ tracts adopt a random coil structure in low concentration. 2) The longer polyQ tract has multiple cooperative binding sites that greatly enhance its binding affinity to the antibody. This aberrant binding affinity could be the reason of Huntingtin protein aggregation. 3) The formation of β-strand or β-sheet structure occurs when peptide concentration exceeds 10 uM. Once a critical concentration is reached, the polyQ tracts begin to nucleate and form aggregates. 4) Lag times and critical concentrations decrease with increasing chain lengths.

We predict that FRET efficiencies of CFP-Qn-YFPs will greatly decrease upon the binding of antibody MW1 Fv. In this way, Fv can break apart the aggregates and stabilize polyQ tracts when they are in an extended conformation. This new information could be used to develop a therapeutic antibody for Huntington's disease. Since the longer polyQ tracts contain multiple binding sites, the covalent linkage of Fv can

produce a new bivalent or multivalent compound with high avidity and specificity for pathologic soluble polyQ tracts. This approach would greatly reduce the potential disruption of other normal polyQ tract containing proteins.

Besides the antibodies, trehalose is another compound used in preventing Htt aggregation. Trehalose is a natural disaccharide synthesized by fungi, plants and invertebrate animals. Trehalose interacts with the expanded polyglutamine tract of the proteins, stabilizing polyQ structure and inhibiting protein aggregation at the initial stage of aggregate formation (Tanaka et al., 2004). Based on Tanaka's work, trehalose is now a lead compound for cure in Huntington's disease patient and has potential for delaying onset or decreasing progression rate in this disease. In the future, it would be interesting to study the binding interaction of trehalose and polyQ tract using the existing CFP-Qn-YFP system. We can also try to co-crystallize of trehalose and polyglutamine peptides.

In addition, the flanking polyproline sequence has been shown by other groups to attenuate the cytotoxicity of polyQ tract in *Saccharomyces cerevisiae*. It is also suggested that the polyproline region may regulate Huntingtin protein conformation to influence its aggregation and subcellular localization (Qin et al., 2004). To examine the effect of the flanking polyproline sequence, we successfully crystallized Fv/Q10P10 complex and determined the structure with molecular replacement with Fv as a search model. Compared the structure of Q10P10 peptide with Q10 peptides, the overall structure of polyQ tract shows the same features as Q10 bound to Fv: Gln 2, 4, 8, 10 have the dihedral angels of a PPII like helix, while Gln 5-7 form a short β-strand to interrupt this PPII helical structure. Thus, the flanking polyproline does not confer structural stability to polyQ tract as expected. The polyproline region is conformational constraint into PPII helix. This finding agrees with circular dichroism spectroscopy data, in which polyproline peptide shows a PPII like helical structure (Darnell et al., 2007). An ideal PPII helix has backbone dihedral angles (φ,ψ) = (-75°, +145°), resulting in precisely three residues per turn. PPII helix is often observed in turns, most commonly in the first residue of a type II β-turn and also in unfolded proteins. PPII helices are specifically bound by the SH3 domain; this binding is important for many protein-

protein interactions. The deletion of polyproline might affect Huntingtin structure and Huntingtin interaction with binding partners, like Grb2 and RasGAP in the Ras-dependent signaling pathways (Liu et al., 1997).

In summary, this study characterizes the structural features of soluble polyglutamine and polyproline peptides in the N-terminal of Huntingtin protein. Our finding provides useful information to elucidate pathologic mechanism of Huntington's disease and contributes to antibody engineering for this disease.

Toll-like Receptor Signaling Pathway

The second part of this thesis focuses on the Toll-like receptor signaling pathway. Firstly, we wanted to study the recruitment of the adaptor protein- MyD88 to TLR through the TIR/TIR domain interaction. TIR domains of TLR1 and TLR2 show the same canonical structure: five β-strands form the core surrounded by five α-helices on both sides and five loops that connect between each β-strands and α-helices. It is interesting to study how MyD88 acts as a universal adaptor for most of the TLRs. We constructed TIR domain of MyD88 and TLRs, including TLR1, 2, 3, 4, 5, 7 and 9 in a pET28 vector and expressed the recombinant proteins in *E.coli*. Unfortunately, none of the recombinant proteins had good solubility and stability. We also constructed pBAC TIR domain expression vector and transfected Sf9 insect cells with baculovirus. Although this baculovirus-assisted insect cell expression system has the advantage of post-translational modification and proper protein folding, we were still unable to produce soluble TIR domain proteins. Co-infection of MyD88 TIR domain and TIRAP TIR domain into Sf9 cells did not improve protein yield and stability. In the future, it should be possible to construct a fusion protein, with linker region connecting TLR1 or TLR2 TIR domain and MyD88 TIR domain to solve this problem. The adjacent TLR1 or TLR2 TIR domain should bind with MyD88 TIR domain and stabilize it in the TIR/TIR domain complex.

The DD superfamily is one of the largest and most widely distributed domain superfamillies. DD superfamily inserts its domain into various signal transduction

proteins such as caspase, kinases, and adaptor proteins. MyD88 is the only adaptor that contains both the DD and TIR domain in the TLR signaling pathway. Site mutagenesis reveals that electrostatic interaction of helix 2 in death domain of MyD88 is responsible for self-assembly. Single mutation from Arginine 62 to Serine could break apart MyD88 death domain oligomers. Two mutations introduced into the MyD88 death domain (E52QR62S) result in a monomeric form of the protein. Results from a GST-pull down experiment suggest that the double mutation does not affect the binding between MyD88DD and IRAK4DD. Far UV circular dichroism spectra indicate that the MyD88 death domain mainly consists of α-helices. This is consistent with our secondary structure prediction, in which the MyD88 death domain is a six helices bundle.

To study the interaction of MyD88 death domain and IRAK4 death domain, we set up protein crystallization with a 1:1 protein mixture. Several crystallization trials were conducted at different temperatures or with different crystallization solutions. Our attempt to crystallize MyD88DD/IRAK4DD complex failed for unknown reasons. An alternative approach to identify the residues involved in MyD88DD and IRAK4DD binding is NMR spectroscopy. The HSQC spectrum shows well dispersed cross peaks for the ^{15}N-MyD88DD double mutant. This indicates that this protein is folded and could be a good candidate for structure determination by NMR. HNCACB and CBCACONH could be collected to assign the residues. Titration MyD88DD with IRAK4DD and mapping the chemical shift would help us to identify the residues on the binding interface.

Beside MyD88DD and IRAK4DD interaction, MyD88DD oligomerization is also important for TLR signaling. The self-assembly of the death domain is a common feature in the death domain suprfamily. A recent publication shows the crystal structure of the oligomeric PIDDosme core complex comprised of seven RAIDD death domains and five PIDD death domains (Park et al., 2007b). This complex uses an asymmetric assembly mechanism and has eight unique interfeaces. In the future it will be interesting to determine whether the MyD88 death domain forms similar platform to mediate TLR signaling. For this purpose, the MyD88 DD oligomer (> 600 kDa) by electron

microscopy to find out the packing pattern of the molecules. A crystallization trial for wild type MyD88 death domain can also be pursued.

The ubiqiutin-protesome plays a crucial role in TLR signalling activation. Pellino1 is a newly identified E3 ubiquitin ligase. In vitro ubiquitination assays show that Pellino1 catalyzes K63-linkage ubiquitination on IRAK1 in the presence of Ubc13/Uev1a complex. Pellino1 contains two CHC2 RING motifs and each of them coordinates with one zinc atom. This tandom arrangement of two RING motifs are different from all other known E3 ligases. To elucidate the mechanism of IRAK1 ubiquitination, we expressed and purifed Pellino1, Ubc13 and Uev1a separately. These three proteins were mixed in a 1:1:1 ratio and used for protein crystallization. Needle-cluster shape crystals were found in two conditions. These cystasl were harvested and verified by SDS-PAGE. We optimized crystallization conditions such as pH, precipitant concentration, temperature and protein concentration to generate single crystals. Thus far we have been unable to obtain the single crystals. Other approaches to optimize the crystallization conditions include the following: 1) Additives, which could stop nucleation and may give you fewer, larger crystals. 2) Oil, diffusion can be slowed down by adding a layer of oil on the top of hanging drop well. 3) Seeding, this is used to grow crystals of the same lattice and symmetry from an identical macromolecule. Once the conditions are optimized, X-ray diffraction data can be collected to determine the structure of Ubc13/Uev1a/Pellino1. The structural data accumulating on ubiquitination enzyme complexes are helping to fill in the pieces of the molecular jigsaw puzzles that comprise these protein modification systems. However, there are still very few examples of well-defined recognition motifs in E2/E3 complex within the ubiquitin system, and very little is known about E3 substrate specificity. This study begins to address these issues as well as the many other unresolved mechanistic questions about ubiquitination in the TLR signaling pathway.

REFERENCES

Alexopoulou L, Holt AC, Medzhitov R and Flavell RA (2001) Recgonition of double – stranded RNA and activation of NF-kappa B by Toll-like receptor3. Nature 413:732-738.

Akira S, Uematsu S, and Takeuchi O (2006) Pathogen recognition and innate immunity. Cell 124: 783-801.

Bennett MJ, Huey-Tubman KE, Herr AB, West AP, Ross SA and Bjorkman PJ (2002) A linear lattice model for polyglutamine in CAG-expansion diseases. PNAS 99:11634-11639.

Bhattacharyya A, Tahkur AK, Chellgren VM, Thiagarajan G, Williams AD and Chellgren BW (2006) Oligoproline effects on polyglutamine conformation and aggregation. J Mol Biol 355:524–535.

Brünger AT, Adams PD, Clore GM, DeLano WL, Gros P, Grosse-Kunstleve RW, Jiang JS, Kuszewski J, Nilges M and Pannu NS (1998) Crystallography & NMR system: A new software suite for macromolecular structure determination. Acta Crystallogr D Biol Crystallogr 54:905-921.

CCPN (1994) The CCP4 suite: programs for protein crystallography. Acta Crystallogr D Biol Crystallogr 50:760-763.

Chellgren BW, Miller AF and Creamer TP (2006) Evidence for Polyproline II helical structure in short polyglutamine tracts. J Mol Biol 361:362-371.

Chen YW, Stott K and Perutz MF (1999) Crystal structure of a dimeric chymotrypsin inhibitor 2 mutant containing an inserted glutamine repeat. PNAS 96:1257-1261.

Darnell G, Orgel JP, Pahl R and Meredith SC (2007) Flanking polyproline sequences inhibit beta-sheet structure in polyglutamine segments by inducing PPII-like helix structure. J Mol Biol 374(3):688-704.

Deng L, Deng C, Wang E, Spencer L, Yang A, Braun J, You C, Slaughter C, Pickart and Chen ZJ (2000) Activation of the IkappaB kinase complex by TRAF6 requires a dimeric ubiquitin-conjugating enzyme complex and a unique polyubiquitin chain. Cell 103:351–361.

Dos Remedios CG, and Moens PD (1995) Fluorescence resonance energy transfer spectroscopy is a reliable "ruler" for measuring structural changes in proteins. J Struct Biol 115:175–185.

Dragatsis I, Efstratiadis A, and Zeitlin S (1998) Mouse mutant embryos lacking huntingtin are rescued from lethality by wild-type extra-embryonic tissues. Development 125:1529-1539.

Dunne A, Ejdeback M, Ludidi PL, O'Neill LA and Gay NJ (2003) Structural complementarity of Toll/interleukin1 receptor identity regions in Toll-like receptors and the adaptors Mal and MyD88. J Biol Chem 278:41443–41451.

Dure LS, Landwehrmeyer GB, Golden J, McNeil SM, Ge P, Aizwa H, Hunang Q, Ambrose CM, Duyao MP, Bird ED, DiFiglia M, Gusella JF, MacDonald ME, Penny JB, Young AB and Vonsattel JP (1994) IT15 gene expression in fetal human brain. Brain Res 659:33–41.

Duyao MP, Auerbach AB, Ryan A, Persichetti F, Barnes GT, McNeil SM, Ge P, Vonsattel JP, Guesella JF and Joyner AL (1995) Inactivation of the mouse Huntington's disease gene homolog Hdh. Science 269:407–410.

Faber PW, Barnes GT, Srinidhi J, Chen J, Gusella JF and MacDonald ME (1998) Huntingtin interacts with a family of WW domain proteins. Hum Mol Genet 7:1463–1474.

Förster T (1948) Intermolecular energy migration and fluorescence. Ann Phys 2:55–75.

Hayashi F, Smith KD, Ozinsky A, Hawn TR, Yi EC, Goodlett DR, Eng JK, Akira S, Underhill DM and Aderem A (2001) The innate immune response to bacterial flagellin is mediated by Toll-like receptor 5. Nature 410:1099-1103.

HDCRG (1993) A novel gene containing a trinucleotide repeats that is unstable on Huntington's disease chromosomes. Cell 72: 971-983.

Heil F, Hemmi H, Hochrein H, Ampenberger F, Kirschning C, Akira S, Lipford G, Wagner H, and Bauer S (2004) Species-specific recognition of single stranded RNA via Toll-like receptor 7 and 8. Science 303:1526-1529.

Hemmi H, Takeuchi O, Kawai T, Kaisho T, Sato S, Sanjo H, Matsumoto M, Hoshino K, Wagner H, Takeda K (2000) A Toll-like receptor recognizes bacterial DNA. Nature 408: 740-745.

Jin MS, Kim SE, Heo JY, Lee ME, Kim HM, Paik SG, Lee H and Lee JO (2007) Crystal structure of the TLR1-TLR2 heterodimer induced by binding of a tri-acylated lipopeptide. Cell 130:1071-1082.

Jones L (2000) Huntingtin interacting proteins and their relevance to Huntington's disease etiology. Neurosci News 3:55-63.

Jones TA and Kjeldgaard M (1997) Electron-density map interpretation. Methods in Enzymology 277:173-208.

Kawai T, Adachi O, Ogawa T, Takeda K and Akira S (1999) Unresponsiveness of MyD88 deficient mice to endotoxin. Immunity 11:115-122.

Ko J, Ou S and Patterson PH (2001) New anti-huntingtin monoclonal antibodies: implications for huntingtin conformation and its binding proteins. Brain Res Bull 56:319-329.

Landwehrmeyer GB, McNeil SM, Dure LS, Ge P, Aizawa H, Huang Q, Ambrose CM, Duyao MP, Bird ED, Bonilla E, de Young M, Avila-Gonzales AJ, Wexler NS, Di Figlia M, Gusella JF, MacDonald E, Penney JB, Young AB and Vonsattel JP (1995) Huntington's disease gene: regional and cellular expression in brain of normal and affected individuals. Ann Neurol 37:218–230.

Lasker MV, Gajjar MM, Nair SK (2005) Cutting edge: Molecular structure of the IL-1R associated Kinase-4 Death Domain and its implications for TLR signaling. J Immun 175:4175-4179.

Lathrop RH, Casale M, Tobias DJ, Marsh JL and Thompson LM (1998) Modeling protein homopolymeric repeats: possible polyglutamine structural motifs for Huntington's disease. Proc Int Conf Intell Syst Mol Biol 6:105-114.

Li C, Zienkiewicz J and Hawiger J (2005) Interactive sites in the MyD88 Toll/Interleukin 1 receptor domain responsible for coupling to the IL1 β signaling pathway. J Biol Chem 280 (28):26152-26159.

Li P, Huey-Tubman KE, Gao T, Li X, West AP, Bennett MJ and Bjorkman PJ (2007) The structure of a polyQ-anti-polyQ complex reveals binding according to a linear lattice model. Nat Struct Mol Biol 14: 381-387.

Liu YF, Deth RC and Devys D (1997) SH3 domain-dependent association of huntingtin with epidermal growth factor receptor signaling complexes. J Biol Chem 272:8121–8124.

Lowe LE, Doherty MT, Karahashi H and Ardit M (2006) Ubiquitination and de-uibiqutination: role in regulation of signaling by Toll-like receptors. J Endo Res 12 (6):337-345.

MacDonald ME, Passani L and Hilditch-Maguire P (2001) Huntingtin associated proteins: potential partners in the pathogenesis of Huntington's disease. In Molecular Mechanisms of Neurodegenerative Diseases. Chesselet MF, Ed. (Humana, Totowa, NJ).

MacDonald ME (2003) Huntingtin: alive and well and working in middle management. Sci STKE 207:48.

Masino L and Pastore A (2001) A structural approach to trinucleotide expansion diseases. Brain Res Bull 56:183-189.

Meylan E, Tschopp J and Karin M (2006) Intracellular pattern recognition receptors in the host response. Nature 442:39-44.

Miyawaki A and Tsien RY (2000). Monitoring protein conformations and interactions by fluorescence resonance energy transfer between mutants of green fluorescent protein. Methods Enzymol 327:472-500.

Muzio M, Ni J, Feng P and Dixit VM (1997) IRAK (Pelle) family member IRAK-2 and MyD88 as proximal mediators of IL-1 signaling. Science 278:1612-1615.

Nasir J, Floresco SB, O'Kusky JR, Diewert VM, Richman JM, Zeisler J, Borowski A, Marth JD, Phillips AG and Hayden MR (1995) Targeted disruption of the Huntington's disease gene results in embryonic lethality and behavioral and morphological changes in heterozygotes. Cell 81:811–823.

O'Neill LA and Bowie AG (2007) The family of five: TIR-domain-containing adaptors in Toll-like receptor signaling. Nat Rev Immunol 7:353-364.

Ordureau A, Smith H, Windheim M, Peggie M, Carrick E, Morrice N and Cohen P (2008) The IRAK-catalyzed activation of the E3 ligase function of Pellino isoforms induces the Lys63-linked polyubiquitination of IRAK1. Biochem J 409:43-52.

Otwinowski Z and Minor W (1997) Processing of x-ray diffraction data collected in oscillation mode. Methods Enzymol 276:307-326.

Park HH, Lo YC, Lin S, Wang L, Yang KJ and Wu H (2007a) The death domain superfamily in intracellular signaling of apoptosis and inflammation. Annu Rev Immunol 25:561-86.

Park HH, Logette E, Raunser S, Cuenin S, Walz T, Tschopp J and Wu H (2007b) Death domain assembly mechanism revealed by crystal structure of the oligomeric PIDDosome core complex. Cell 128:533-546.

Passani LA, Bedford MT, Faber PW, McGinnis KM, Sharp AH and Gusella JF (2000) Huntingtin's WW domain partners in Huntington's disease post-mortem brain fulfill genetic criteria for direct involvement in Huntington's disease pathogenesis. Hum Mol Genet 9:2175–2182.

Patterson G, Day RN, and Piston D (2001) Fluorescent protein spectra. J Cell Sci 114:837-838.

Perutz MF, Staden R, Moens L and De Baere I (1993) Polar zippers. Curr Biol 3:249-253.

Pickart CM (2000) Ubiquitin in chains. Trends in Biochem Sci 25(11):544-548.

Pickart CM (2001) Mechanisms underlying ubiquitination. Annu Rev Biochem 70:503-533.

Qin ZH, Wang Y, Sapp E, Cuiffo B, Wanker E and Hayden MR (2004) Huntingtin bodies sequester vesicle-associated proteins by a polyproline-dependent interaction. J Neurosci 24: 269–281.

Ross C (2002) Polyglutamine pathogenesis: emergence of unifying mechanisms for Huntington's disease and related disorders. Neuron 35:819-822.

Rubinsztein DC, Leggo J, Coles R, Almqvist E, Biancalana V, Cassiman J, Chotai K, Connarty M, Crauford D, Curtis A, Crutis D and Davidson M (1996) Phenotypic characterization of individuals with 30-40 CAG repeats in the Huntington's disease(HD) gene reveals HD cases with 36 repeats and apparently normal elderly individual with 36-39 repeats. Am J Hum Genet 59:16-22.

Sambashivan S, Liu Y, Sawaya MR, Gingery M and Eisenberg D (2005) Amyloid-like fibrils of ribonuclease A with three-dimensional domain-swapped and native-like structure. Nature 437:266-269.

Saitoh S, Akashi S, Yamada T, Tanimura N, Kobayashi M, Konno K, Matsumoto F, Fukase K, Kusumoto S, Nagai Y, Kusumoto Y, Kosugi A and Miyake K (2004) Lipid A antagonist, lipid IVa, is distinct from lipid A in interaction with Toll-like receptor 4 (TLR4)-MD-2 and ligand-induced TLR4 oligomerization. Int Immunol 16:961.

Sathasivam K, Amaechi I, Mangiarini L, and Bates GP (1997) Identification of an HD patient with a (CAG) 180 repeats expansion and the propagation of highly expanded CAG repeats in lambda phage. Hum Genet 99:692-695.

Schauvliege R, Janssens S and Beyaert R (2006) Pellino proteins are more than scaffold proteins in TLR/IL-1R signalling: a role as novel RING E3-ubiquitin-ligases. FEBS Lett 580:4697-4702.

Schauvliege R, Janssens S and Beyaert R (2007) Pellino proteins: novel players in TLR and IL-1R signalling. J Cell Mol Med 11:453-461.

Scheffener M, Nuber U and Huibregtse JM (1995) Protein ubiquitination involving an E1-E2-E3 enzyme ubiquitin thioester cascade. Nature 373(6509):81-83.

Scherzinger E, Sittler A, Schweiger K, Heiser V, Lurz R, Hasenbank R, Bates GP, Davies SW, Lehrach H, and Wanker EE (1997) Huntingtin-encoded polyglutamine expansions form amyloid like protein aggregates in vitro and in vivo. Cell 90:549-558.

Sharma D, Sharma S, Pasha S and Brahmachari SK (1999) Peptide models for inherited neurodegenerative disorders: conformation and aggregation properties of long polyglutamine peptides with and without interruptions. FeBS Lett 456:181-185.

Sittler A, Walter S, Wedemeyer N, Hasenbank R, Scherzinger E and Eickhoff H (1998) SH3GL3 associates with the Huntingtin exon 1 protein and promotes the formation of polygln-containing protein aggregates. Mol Cell 2:427–436.

Starikov EB, Lehrach H and Wanker EE (1999) Folding of oligoglutamines: a theoretical approach based upon thermodynamics and molecular mechanics. J Biomol Struct Dyn 17:409-427.

Takeda K and Akira S (2005) Toll-like receptors in innate immunity. Int Immunol 17:1-14.

Takeuchi O, Hoshino K, Kawai T, Sanjo H, Takada H, Ogawa T, Takeda K and Akira S (1999) Differential roles of TLR2 and TLR4 in recognition of the gram-negative and gram-positive bacterial cell wall components. Immunity 11:443-451.

Takeuchi O, Takeda K, Hoshino K, Adachi O, Ogawa T and Akira S (2000) Cellular responses to bacterial cell wall components are mediated through MyD88-dependent signaling cascades. Int Immunol 12:113-117.

Tanaka MY, Machida S, Niu T, Ikeda NR, Jana H, Doi M, Kurosawa M, Nekooki and Nukina N (2004) Trehalose alleviates polyglutamine-mediated pathology in a mouse model of Huntington disease. Nat Med 10(2):148-54.

Tsien RY (1998) The green fluorescence protein. Annu Rev Biochem 67:509-544.

Wang C, Deng L, Hong M, Akkaraju GR, Inoue J and Chen ZJ (2001) TAK1 is a ubiquitin-dependent kinase of MKK and IKK. Nature 412:346-351.

Wang X, Vitalis A, Wyczalkowski MA and Pappu RV (2006) Characterizing the conformational ensemble of monomeric polyglutamine. Proteins 63:297-311.

Wesche H, Henzel WJ, Shillinglaw W, Li S and Cao Z (1997) MyD88: an adapter that recruits IRAK to the IL-1 receptor complex. Immunity 7:837-847.

Xiao T, Towb P, Wasseerman SA, and Sprang SR (1999) Three-dimensional structure of a complex between the death domains of Pelle and Tube. Cell 99: 545-555.

Xu Y, Tao X, Shen B, Horng T, Medzhitov R, Manley JL and Tong L (2000) Structural basis for signal transduction by the Toll/interleukin-1 receptor domains. Nature 408:111–115.

Zeitlin S, Liu JP, Chapman DL, Papaioannou VE and Efstratiadis A (1995) Increased apoptosis and early embryonic lethality in mice nullizygous for the Huntington's disease gene homologue. Nat Genet 11:155-163.

Zhang M, Windheim M, Roe SM, Peggie M and Cohen P (2005) Chaperoned ubiquitylation-crystal structures of the CHIP U box E3 ubiquitin ligase and a CHIP-Ubc13-Uev1a complex. Mol Cell 20:525-538.

Zheng N, Wang P, Jeffrey PD, and Pavletich NP (2000) Structure of a c-Cbl-Ubch7 complex: RING domain function in ubiquitin protein ligases. Cell 102:533-539.

VITA

Name:	Zhuyun Liu
Address:	c/o Dr. Pingwei Li Department of Biochemistry and Biophysics Texas A&M University College Station, TX, 77843-2128
Email Address:	zhuyunliu@tamu.edu
Education:	B.S., Biotechnology, Nankai University, 2005 M.S., Biochemistry, Texas A&M University, 2008